

1 **Abstract**

2 Numerical simulations of a gas-particle-droplet system were performed using an Euler-
3 Lagrange approach. Models accounting for (i) the interaction between droplets and particles,
4 (ii) evaporation from the droplet spray, as well as (iii) evaporation of liquid from the surface
5 of non-porous particles were considered. The implemented models were verified for a packed
6 bed, as well as other standard flow configurations. The developed models were then applied
7 for the simulation of flow, as well as heat and mass transfer in a fluidized bed with droplet
8 injection. The relative importance of droplet evaporation vs. evaporation from the particle
9 surface was quantified. It was proved that spray evaporation competes with droplet deposition
10 and evaporation from the particle surface. Moreover, we show that adopting a suitable surface
11 coverage model is vital when attempting to make accurate predictions of the particle's liquid
12 content.

13 **Keywords:** Fluidized bed granulation, wet granular matter; CFD-DEM simulation; Euler-
14 Lagrange simulation

15

1 Introduction

2 In various industries such as the petrochemical or the food & pharmaceuticals sector,
3 granulation and agglomeration processes are of key importance. Often, granulation processes
4 are used to stabilize an intermediate or final product, or change product properties, by means
5 of the addition of a liquid binder. Consequently, it is essential to consider wetting, drying,
6 particle shaping and size enlargement, as well as the homogenization of the product. Fluidized
7 beds are one of the promising tools to integrate all of these features into a single process step,
8 mainly due to the high rate of heat and mass transfer in these devices.¹

9 Various phenomena occur in fluidized bed granulators: i) deposition of droplets on the
10 particle surface due to particle-droplet collisions; ii) evaporation of liquid from the particle
11 surface stemming from the flow of heated gas over the wet particles; and iii) particle
12 agglomeration due to the collision of wet particles. In addition, fluidized beds are
13 characterized by spatio-temporal fluctuations of the flow quantities (e.g., the local particle
14 concentration, the fluid and particle velocity, as well the concentration of vapor or
15 temperature). Since these phenomena are coupled, the overall behavior of a fluidized bed
16 granulator is complex. A variety of approaches for their analysis, of which (i) compartment
17 models, as well as (ii) detailed models based on computational fluid dynamics (CFD) are the
18 most important ones.

19 A comparably large number of researchers use compartment (or zone) models, which strongly
20 simplify the system by utilizing a compartment for each phenomenon. The compartments
21 typically comprise²: 1) a spray or wetting zone in which droplets and particles interact³; 2) a
22 drying zone in which evaporation from the particles' surface takes place; 3) a non-active zone
23 in which bed temperature and gas humidity fluctuate marginally; and 4) a heat transfer zone,
24 where particles are heated by fluidization gas. These compartment models have been
25 extensively applied for population balance modeling by various researchers, often with good
26 success.⁴⁻⁹ However, the size of the above mentioned zones are often estimated, and their

1 geometry is based on a number of simplifications: for instance, Link et al. ¹⁰ considered the
2 spray zone as a bi-conical region whose size is defined by the injection depth of the jet and
3 spray angle. Fries et al. ¹¹ used a bi-conical zone to estimate the particle residence time
4 distribution in the spray region. Maronga, Wnukowski ² obtained the temperature and gas
5 humidity distributions experimentally to estimate the above mentioned regions. Börner et al.
6 ¹² used a conductivity probe to define the wetting zone and the drying zone in a fluidized bed.
7 Lower attention was given in previous years to CFD-based models, since the precision of the
8 used model is still fairly low and typical calculation times are in the order of days or even
9 weeks. For example, Sutkar et al. ¹³ performed CFD-DEM simulations and considered
10 droplets as discrete particles. This previous work used a wet restitution coefficient to account
11 for droplet-particle interactions. Unfortunately, the evaporation from the spray droplets, and
12 droplets deposited on the particle surface were disregarded in their study. In addition, in the
13 study of wet fluidized bed, the non-uniformity of the droplet distribution on the particle
14 surface was not considered in most studies. However, this non-uniformity plays an important
15 role in the rate of evaporation from the particle surface: Štěpánek, Rajniak ¹⁴, were one of the
16 first that provided a model for liquid spreading (i.e., a model for “surface coverage”) on the
17 particle surface that helps to quantify this effect. While previous modeling approaches were
18 limited, experimental studies presented in the open literature¹⁵⁻¹⁷ are also faced with several
19 constrains in providing local information that could help to clarify the roles of the evaporation
20 phenomena.

21 Having considered the above studies, it can be concluded that more research seems necessary
22 to better understand the phenomena in a wet fluidized bed. In the current contribution we aim
23 on a purely numerical approach relying on a rigorous CFD-based model. This is motivated by
24 the inability of experimental techniques to provide local information on phase change
25 phenomena (e.g., evaporation). We believe that such a numerical approach, once carefully
26 verified, can be a key tool to probe local phenomena. This is true at least for situations where

1 particles are approximately spherical, have the same size and density, and the system size
2 allows a direct simulation of (primary) particle motion (with primary particles we refer to
3 individual solid bodies in contrast to meso-particles, which can be constituted by multiple
4 primary particles connected by some type of cohesive forces). Exactly this is true for the
5 simulation approach chosen in this work, i.e., the employed CFD-DEM, which has been used
6 with increasing frequency in the recent past by Zhu et al. ¹⁸, Radl et al. ¹⁹, Girardi et al. ²⁰,
7 Van Buijtenen et al. ²¹, and Sutkar et al. ¹³. In the present contribution we significantly extend
8 these previous studies by analyzing the distribution of the gas temperature, the liquid content
9 of the particles and the air, as well as the gas humidity. This understanding can be used for a
10 more profound determination of the various zones in the fluidized bed relevant for the widely-
11 used compartment models. Moreover, CFD-DEM simulations allows to extract useful data
12 related to particle-particle (or particle-wall) impact velocities, particles collision angle
13 distribution, or the granular temperature. These data can be utilized in the development of
14 aggregation kernels to be applied in the population balance equation for meso-particle (i.e.,
15 agglomerates). Again, this motivates the present study which focuses on a quantification of
16 temperature, vapor and liquid distribution in a fluid bed wet granulator.

17 The overall modeling strategy employed in the present work is as follows: we first
18 implemented all necessary models in the frame of the CFDEM[®] code to simulate particle-
19 droplet-fluid interaction in a fluidized bed. In order to keep the model complexity (and hence
20 the number of parameters) low, we focus on non-porous particles. While such particles
21 represent only a small fraction of industrially-relevant systems, this choice allows us to isolate
22 gas-side from intra-particle influence parameters. Furthermore, cohesive inter-particle forces
23 due to liquid bridges were neglected on purpose in the present contribution: we will see that
24 this is justified by the very low liquid content of the particles in our simulations. Second,
25 routines that allows us to perform a local analysis of all relevant phenomena (e.g., droplet
26 deposition, or evaporation) were implemented in CFDEM[®]. Third, an array of two-

1 dimensional, and explorative (because computationally very expensive) three-dimensional
2 simulations were performed in a bubbling fluidized bed with liquid injection. Interestingly,
3 we find from all of these simulations that particles are wet only in a very small region of the
4 fluidized bed. Thus, cohesive liquid bridge forces will only be relevant in a small fraction of
5 the particle bed, which is in sharp contrast to previous work which often assumed a uniform
6 liquid distribution (e.g., as assumed in Girardi et al.²⁰ or Sutkar et al.¹³). It is clear that the
7 reason for this is liquid evaporating from the particle surface and the droplet suspended in air
8 – these phase change phenomena obviously play a key role in the overall dynamics of the wet
9 particle bed. Fluid and particle cooling induced by evaporation has been ignored in all
10 relevant previous studies^{13,20} we are aware of. This is despite the fact that these cooling effects
11 can affect the distribution of moisture and temperature in the bed, making predictions of, e.g.,
12 liquid bridge volume extremely difficult. We will show by an analysis of the rate of
13 evaporation from the droplets, as well as from on the particle surface, the origin of this
14 finding. Furthermore, and to the best of our knowledge, we are the first that quantify in detail
15 the effect of evaporative cooling on the bed behavior. We believe that these pieces of
16 information are of critical importance for the development of simplified models required for a
17 fast estimation of granulation process dynamics, or process control. It should be noted that
18 the present work mainly focuses on gas-particle-droplet interaction in a bubbling fluidized
19 bed. Consequently, the injection velocity was chosen lower than in typical industrial
20 applications to preserve the bubbling characteristics. This leads to longer the droplet-in-
21 suspension time scales, and hence droplet evaporation is more pronounced in our present
22 study than in a typical industrial application. In addition, the assumption of non-porous
23 particles over-emphasises evaporation from the particle surface. These facts lead to low LoD,
24 and hence agglomeration would be unlikely to occur in our simulations. Consequently, more
25 research effort would be required to eliminate these constrains so that reasonable LoD values
26 can be predicted, and a real-world fluidized bed granulator can be simulated. This is clearly

1 beyond the current focus, and hence we restrict the current study to systems without
2 agglomeration and low liquid contents.

3 Our paper is structured as follows: in the following Section, the governing transport
4 equations, as well as the constitutive equations used for simulation of heat and mass exchange
5 will be described. In the third section, the result of a grid sensitivity study will be presented,
6 followed by an analysis of the effect of model details and operating conditions. Finally, in the
7 last section, the main findings of the present study are viewed in the context of available
8 literature, and some thoughts on future research activities are presented.

9 **Mathematical Modeling**

10 In the present study, simulations were performed utilizing an extended version of the
11 CFDEM[®] code.²² This code is based on an open-source CFD–DEM framework to simulate
12 coupled fluid–particle systems. The motion of the particles is resolved by means of the DEM
13 and simulated using the LIGGGHTS[®] code.²³ The interstitial fluid flow is resolved through
14 CFD and simulated using the OpenFOAM[®] code.²⁴ Key additions to CFDEM[®] by us include
15 (i) a framework for tracking an arbitrary number of species (and the temperature) in the gas
16 phase, as well as (ii) evaporation models. A brief description of the governing equations for
17 the above transport phenomena is presented next.

18 **Fluid Phase**

19 Momentum equation for the fluid phase (assumed to consist of air, vapor, and the suspended
20 droplets) is solved based on the well-known Navier-Stokes equation:

$$\frac{\partial}{\partial t}(\mathbf{u}_f \varphi_f \rho_f) + \nabla \cdot (\mathbf{u}_f \mathbf{u}_f \varphi_f \rho_f) = -\varphi_f \nabla \cdot \boldsymbol{\tau}_f - \varphi_f \nabla P_f + \boldsymbol{\Phi}_d + \varphi_f \rho_f \mathbf{g} \quad (1)$$

21 Note that the fluid density and viscosity is assumed to be constant and equal to that of air, i.e.,
22 we do not consider the effect of suspended droplets and vapor on the fluid’s momentum
23 balance. This is justified by the low mass loading (and the very small volume concentration)

1 of droplets and vapor in the system. Specifically, one might want to compute an expected
 2 (combined) mass loading of droplet and vapour from the injected amount of liquid and the
 3 mass inlet rate of the fluidizing gas $(\mu_{liq} + \mu_{vap})_{expected} = \dot{S}_{inj} V_{inj} / u L_{bed} w_{bed} \rho_g$. Here
 4 V_{inj} is the volume of the injection region. As long as this expected mass loading is much
 5 smaller than unity (one might adopt 0.1 as a threshold), our assumption of negligible effects
 6 on the fluid's momentum transport equation will be valid to a first approximation. This is the
 7 case for all situations considered in the present study.

8 The term Φ_d is the force exerted by particles on fluid phase per unit volume, excluding
 9 buoyancy effects. In line with previous work and the current understanding in the field, it was
 10 assumed that the drag force is the main force contributing to the momentum exchange
 11 between gas and particles. These drag forces can be computed using the correlation developed
 12 by Beetstra et al.²⁵ as follows:

$$\Phi_d = -\beta_{sf}(\mathbf{u}_f - \mathbf{u}_p) \quad (2)$$

$$\beta_{sf} = 18\rho_f \nu_f \varphi_f (1 - \varphi_f) \frac{F(\varphi_f, Re)}{d_p^2} \quad (3)$$

$$F(\varphi_f, Re) = 10 \frac{1 - \varphi_f}{\varphi_f^2} + \varphi_f^2 \left(1 + 1.5 \sqrt{1 - \varphi_f} \right) + \frac{0.413 Re \left(\frac{1}{\varphi_f} + 3\varphi_f(1 - \varphi_f) + 8.4 Re^{-0.343} \right)}{24\varphi_f^2 \left(1 + 10^{3(1-\varphi_f)} Re^{-\frac{1}{2}(1+4(1-\varphi_f))} \right)} \quad (4)$$

13

14 **Particles**

15 The motion of individual particles is solved using Newton equation of translational and
 16 rotational motion:

$$\rho_{p,i} V_{p,i} \frac{\partial \mathbf{u}_{p,i}}{\partial t} = \mathbf{f}_{cont,i} + \beta_{sf} V_{p,i} (\mathbf{u}_f - \mathbf{u}_{p,i}) - V_{p,i} \nabla P_{f,i} + \mathbf{g} \quad (5)$$

$$I_{p,i} \frac{d}{dt} \omega_{p,i} = \mathbf{t}_i \quad (6)$$

1 Where the forces exerted on the particles, and shown on the right hand side of the above
 2 equation, include (i) contact, (ii) drag, (iii) far field pressure, and (iv) gravity respectively.
 3 Due to the minute amounts of liquid in the system, we assume that both (i) density and (ii)
 4 mass of the particles are invariant with time. The contact law is based on a Hertzian
 5 interaction model with tangential history tracking. The contact forces in the normal and
 6 tangential direction are respectively given by

$$\mathbf{f}_{cont,i,n} = -k_n \delta_p + \eta_n \Delta u_{i,n} \quad (7)$$

$$\mathbf{f}_{cont,i,t} = \min \left\{ \left| k_t \int_{t_{c,0}}^t \Delta u_{i,t} dt + \eta_t \Delta u_{i,t} \right|, \mu_c \mathbf{f}_{cont,i,n} \right\} \quad (8)$$

7 Here δ_p denotes the particles overlap; k and η represent the stiffness coefficient and damping
 8 factor, respectively. These parameters can be calculated as a function of the Young modulus
 9 Y , the Poisson ration ν , and the coefficient of restitution e . The values of these parameters, as
 10 well as of the friction coefficient are reported in Table 2. More details regarding the adopted
 11 models can be found on the LIGGGHTS® online documentation²⁶
 12 (<http://www.cfdem.com/media/DEM/docu/Manual.html>)

13 **Mass and Heat Transfer**

14 Due to the temperature difference between the fluid phase, the injected droplets, and the
 15 particles, as well as evaporation phenomenon, it is necessary to solve heat and mass transport
 16 equations for all relevant species in this system. A key phenomenon is the depletion of the
 17 local droplet content due to evaporation. Thus, the transport equation of for the local droplet
 18 mass loading needs to be considered, which reads:

$$\begin{aligned} \frac{\partial}{\partial t}(\mu_{liq}\varphi_f\rho_f) + \nabla \cdot (\mathbf{u}_f\mu_{liq}\varphi_f\rho_f) - \nabla \cdot (D_{eff}\nabla(\mu_{liq}\varphi_f\rho_f)) \\ = -\dot{S}_{evap,f} - \dot{S}_d + \dot{S}_{inj} \end{aligned} \quad (9)$$

1 Here μ_{liq} is the mass loading of the droplet in the gas phase (i.e., the mass of droplets divided
2 by the mass of the gas phase), which equals $\frac{C_{liq}}{\varphi_f\rho_f}$; $\dot{S}_{evap,f}$ is the sink term for evaporation of
3 the spray in the gas phase; \dot{S}_d is the rate of droplet deposition on the particle bed, and \dot{S}_{inj} is
4 the source term due to the injection of liquid droplets. The method used for the calculation for
5 these source and sink terms will be described later.

6 The transport equation for the mass loading of any gas-phase species, in our case water vapor,
7 considering phase change phenomena is given by:

$$\frac{\partial}{\partial t}(\mu_{vap}\varphi_f\rho_f) + \nabla \cdot (\mathbf{u}_f\mu_{vap}\varphi_f\rho_f) - \nabla \cdot (D_{eff}\nabla(\mu_{vap}\varphi_f\rho_f)) = \dot{S}_{evap,f} + \dot{S}_{evap,p} \quad (10)$$

8 Here the term $\dot{S}_{evap,p}$ is the rate of evaporation from the particle surface.

9 A lumped transport equation for the thermal energy of the fluid phase (i.e., air, vapor and
10 suspended droplets) can be derived, which is:

$$\begin{aligned} \varphi_f\rho_f C_{p,f} \frac{\partial T_f}{\partial t} + \nabla \cdot (\mathbf{u}_f\varphi_f\rho_f C_{p,f} T_f) - \nabla \cdot (\lambda_{eff}\nabla(\varphi_f T_f)) \\ = -ha_p(T_f - T_p) - \dot{S}_{evap,f}\Delta H_{evap} \end{aligned} \quad (11)$$

11 The first term on the right hand side of the above equation is the volume-specific rate of heat
12 exchange between the gas phase and the particles. The second term is the sink term due to
13 evaporation of the droplets suspended in the gas phase. Again, we assume that the fluid
14 density and heat capacity is constant and equal to that of air, motivated by the low mass
15 loading of droplets and vapor in the system.

1 Closure for the Heat Transfer Rate

2 Parameter h in Equation 11 is the heat transfer coefficient, which can be calculated via the
3 Nusselt number correlation developed by Deen et al.²⁷ for the fluidized bed. Thus, we use the
4 following Nusselt number correlation to compute h :

$$Nu = (7 - 10\varphi_f + 5\varphi_f^2)(1 + 0.7Re^{0.2}Pr^{1/3}) + (1.33 - 2.4\varphi_f + 1.2\varphi_f^2)Re^{0.7}Pr^{1/3} \quad (12)$$

5 Here Re is calculated based on the superficial fluid-particle relative velocity; Nu is defined
6 as $(h d_p)/\lambda_f$. Correspondingly, the equation of heat transfer from or to a single particles is:

$$m_p C_{p,p} \frac{\partial T_p}{\partial t} = hA_p(T_f - T_p) - \dot{S}_{evap,p}\Delta H_{evap} \quad (13)$$

7 Note, that the heat of evaporation from the droplets deposited on the particles is taken into
8 account on the particle side only. Thus, evaporation from the particle surface will indirectly
9 affect the fluid's temperature via the coupling of the thermal transport equations of the fluid
10 and particle phase.

11 Closure for Droplet Evaporation and Liquid Deposited on the Particle Surface

12 In this study, the rate of droplet evaporation on the particle surface was calculated based on
13 the driving force for transfer of water vapor between the particle and the gas phase. This rate
14 was computed using the saturation density of water vapor at the particle temperature $\rho_{w,Sat}$
15 as

$$\dot{S}_{evap,p} = |\rho_{w,Sat} - \rho_g \mu_{vap}| a_{dp} \beta \quad (14)$$

16 Here β is the mass transfer coefficient which can be calculated based on Sherwood number
17 defined as $Sh = (\beta d_p)/D_{vap}$. This coefficient has been calculated in analogy to the heat
18 transfer coefficient correlation developed by Deen et al.²⁷ shown in Eqn. 12. It should be
19 noted that this correlation condenses to the correct limit (i.e., $Nu = Sh = 2$) for no slip (i.e.,

1 $Re = 0$) and an infinitely dilute system (i.e., $\varphi_f = 1$). Hence, we use the same symbol, i.e.,
 2 β , for denoting the mass transfer coefficient from the particles and the droplet cloud.
 3 Specifically, β is assumed to be constant for all droplets, and $Sh = 2$. This is a realistic
 4 assumption, since the droplet volume concentration is very low, and droplets are quickly
 5 deposited on particles (i.e., the dependency of Sh and β on φ_f shown in Eqn. 12 is assumed to
 6 be irrelevant for the droplets; droplets share the same speed as the air).

7 In Eqn. 14, $\rho_{w,sat}$ can be estimated based on ideal gas law and the Antoine Equation for the
 8 vapor pressure of water; a_{dp} is the surface area of the particle that is wetted by the droplets,
 9 and hence available for liquid evaporation. Due to the fact that this area is the most difficult
 10 parameter to estimate when calculating the particles' evaporation rate, two models were
 11 implemented in the code and investigated. The first model assumes that the surface
 12 coverage ψ_{liq} , defined as the ratio of the surface area available for evaporation and the
 13 surface area of the particle, is linearly related to the dimensionless liquid content as follows:

$$\psi_{liq} = \max(0, L_p^* - L_{p,noevap}^*) \quad (15)$$

14 Here L_p^* and $L_{p,noevap}^*$ are the volume fraction of liquid on the particle, and a threshold value
 15 below which evaporation from the particle surface is impossible, respectively.

16 The second model considered is that developed by Kariuki et al. ²⁸, in which the surface
 17 coverage is calculated as

$$\psi_{liq} = 1 - [1 - f]^{\Phi_p/f} \quad (16)$$

18 Where the parameter f is the fraction of the particle surface coated by a single droplet, and
 19 Φ_p is the particle coating number given by

$$f = \frac{A_{d,projected}}{A_p} = \frac{\frac{\pi}{4} d_d^2}{\pi d_p^2} = \left(\frac{d_d}{2d_p} \right)^2 \quad (17)$$

$$\Phi_p = N_d f \quad (18)$$

1 For the calculation of the rate evaporation of liquid droplets suspended in air the same
2 methodology as for the evaporation from the particle surface was adopted, i.e.

$$\dot{S}_{evap} = |\rho_{w,sat} - \rho_g \mu_{vap}| \varphi_{liq} a_d \beta \quad (19)$$

3 Where $\rho_{w,sat}$ is the saturation density of water vapor in the gas phase at the gas temperature;
4 φ_{liq} is the volume fraction of liquid water in the gas phase; and a_d is the specific surface area
5 of a single droplet given by $a_d = \frac{6}{d_d}$.

6 Closure for Droplet Deposition

7 In order to simulate the deposition of droplets on the particle surface, a clean-bed filter model
8 was adopted from the work of Kolakaluri²⁹. Through direct numerical simulation of flow
9 through a packed bed, he developed a correlation for the filtration coefficient as a function of
10 the particle Reynolds Number, the droplet Stokes Number, and the solid volume fraction²⁹. In
11 his model, droplet deposition rate can be calculated as

$$\dot{S}_d = -\lambda |\mathbf{u}_d - \mathbf{u}_p| \mu_{liq} \varphi_f \rho_f \quad (20)$$

12 Where $|\mathbf{u}_d - \mathbf{u}_p|$ is the slip velocity between the fluid phase and the particle. The equations
13 required for calculation of the filtration coefficient are summarized in Table 1. It should be
14 noted that the effective droplet Stokes Number St_{eff}^* is calculated based on the true slip
15 velocity, while the mean particle Reynolds Number is calculated using superficial velocity.
16 Thus, we assume that droplets have the same (average) speed as the gas phase. This is
17 justified due to the small droplet diameter, resulting in a very small relaxation time (i.e., ca.
18 $1.2 \cdot 10^{-3}$ [s]) of the droplets.

19 *Table 1*

1 After successful implementation and verification (see Appendix A) of the above-mentioned
2 models, more than twenty sets of simulations were performed in order to examine the effect
3 of model details and operation conditions. The results of these simulations will be thoroughly
4 explained in following section.

5 **Results and Discussion**

6 In the wet fluidized bed, due to the interaction among particle, droplet, and fluid, an integral
7 study of such a system appears to be a complex task. Therefore, in this section, the effect and
8 contribution of each phenomenon has been investigated in an isolated manner first. The
9 simulation set up as well as physical properties and simulation condition for the studied
10 system has been presented in Figure 1 and Table 2. It should be noted that particles and
11 droplet specifications, as well as operating conditions have been adopted based on a certain
12 industrial application and the experience of our research institute. For instance, the droplet
13 size of $20\ \mu\text{m}$ was chosen, which is a typical size in an industrial application.

14 *Figure 1*

15 Droplets are sprayed on the particles from the top considering the injection zone. The size of
16 this region was defined such that the relative amount of injected droplets in this region
17 (compared to the particle mass) equals the corresponding value in a typical fluidized bed
18 granulator. Gas and particles are initially considered having the same temperature.

19 It should be noted that in order to be able to study the bed behavior in bubbling regime, the
20 liquid injection velocity was set to ca. 2 times the fluidization velocity. This is not
21 representative of most industrial applications since in industrial systems the spray injection
22 velocity is chosen often very high, i.e., in the order of 10 [m/s]. Such a high injection velocity
23 would destroy the typical fluidization behavior of the particles, and would lead to two large
24 recirculation zones in our simulations. Since our simulation domain only represents a small

1 fraction of a real-world fluidized bed, these recirculation zones are not representative of most
2 industrial applications.

Table 2

3 Simulations were performed for 50s real time for all cases. It took approximately three days
4 on 6 cores of a XEON workstation (Intel® Xeon® CPU “X5680”, 3.33 GHz) to complete
5 each 2D case (i.e., approximately 400 CPUhrs/case). For the 3D case we used 32 cores of
6 dcluster.tugraz.at (i.e., a double octo-core cluster relying on Intel® Xeon® “E5-2650” CPUs,
7 2.0 GHz, InfiniBand Interconnect) for ca. 20 days per case (i.e., approximately 15,000
8 CPUhrs/case).

9 **Grid Sensitivity Study**

10 In order to investigate the independency of the solution on the mesh, several simulations were
11 performed for grid sizes of $1.5 d_p$, $2 d_p$ and $3 d_p$. For the finest grid size, a smoothing model
12 was used to smooth all exchange fields (e.g., the particle volume mapped to the fluid grid)
13 with the smoothing length of $2 d_p$. As discerned from Figure 2, refining the computational
14 domain to a value smaller than $2 d_p$ does not improve the accuracy of results for mass
15 loadings and gas temperature. For the grid size of $3 d_p$, small deviations can be observed,
16 especially for the gas temperature and the vapour mass loading near the bed outlet, as well as
17 the spray region. As a result, the grid size of $2 d_p$ was adopted to achieve high accuracy and
18 low computational cost.

19 *Figure 2*

20 **Effect of Model Details**

21 During the interaction of the three phases (i.e., particles, droplets, and the fluid) in the
22 fluidized bed, a number of phenomena need to be taken into account: for example, the
23 evaporation of the injected liquid will reduce the particles’ temperature, which will change the

1 driving force for evaporation. In this section, the role of these phenomena including (i) droplet
2 deposition, (ii) the evaporation from the spray's droplet and (iii) from the particle surface in
3 the bed will be studied. This will be done both independently and in connection with other
4 phenomena. In addition, the effect of different models for evaporation from particle surface is
5 evaluated.

6 *Table 3*

7 The Effect of Involved Phenomena

8 The contributions of involved phenomena have been investigated through simulation of four
9 cases according to Table 3. It should be mentioned that in Case B, no droplet deposition and
10 zero initial LoD will result in no evaporation of liquid from the particles' surface.

11 *Figure 3*

12 Comparing the exchange rates in Figures 3a-c demonstrates that the rate of spray evaporation
13 is two orders of magnitude larger than the rates of droplet deposition and evaporation from
14 particle surface. Thus, the spray evaporation is hardly affected by particle-related phenomena
15 in Cases A-C. Nonetheless, in the case of no spray evaporation, i.e. Case D, the deposition
16 rate is 2 orders of magnitude higher in comparison to its rate in the case with spray
17 evaporation. This proves that droplets are consumed due to the deposition since both
18 phenomena depend on droplet concentration. In addition, upon neglecting spray evaporation,
19 the rate of evaporation from the particles increases. This is due to a lower vapor mass loading,
20 and consequently the higher driving force for evaporation. It can be concluded that the
21 evaporation from suspended droplets (i.e., the spray) competes against the droplet deposition
22 on one hand, and the evaporation from the particle surface on the other hand.

23 Regarding the phenomena occurring on the particle surface in Cases A and C, it can be clearly
24 seen that the deposition rate is not influenced by evaporation from the particle surface. This is

1 due to the fact that the main driving force for deposition is the liquid mass loading in the air.
2 Also, it can be seen from Figures 3a that the rate of deposition and evaporation from the
3 particle surface match each other (in a time-average sense) after a few seconds. Thus, the rates
4 of deposition and evaporation adjust rather quickly to their quasi steady state values. At such
5 a quasi-steady state, particle deposition and evaporation rates must match each other, since the
6 particles were assumed to be non-porous in the present study. Clearly, for Case C (in which
7 we model deposition, but no evaporation from the particle surface) we expect a slow increase
8 of the particles water content, which is confirmed by our data shown in Figure 4c.

9 *Figure 4*

10 Another point discerned from Figure 3 is that the droplet deposition rate fluctuates strongly,
11 i.e., by two orders of magnitude. This is explained by the bubbling nature of the fluid bed
12 granulator, and the fact that the deposition rate strongly depends on the local solid volume
13 fraction.

14 *Table 4*

15 In order to compare the exchange rates in a more quantitative way, the integral exchange
16 rates, normalized with liquid injection rate, have been presented in Table 4. Thereby,
17 normalized quantities are indicated by an asterisk. These rates have been time-averaged over
18 the last 30 second of simulation time, in which the flow was already in the quasi steady state.
19 The mass is conserved in all cases for both liquid and vapor within a maximum error of
20 1.92% (see rightmost column). As mentioned before, almost matching rates of deposition and
21 evaporation from the particle surface are predicted. However, the droplet evaporation is
22 clearly the dominant phenomenon in the studied cases. In case this phenomenon is not
23 considered, only 11% of the liquid evaporates, and significant mass losses are induced (see
24 the significant increase in the dimensionless liquid mass flow at the outlet).

1 To gain a deeper insight into the contribution of the investigated phenomena, an analysis via
 2 characteristic time scales can be useful. Unfortunately, such an analysis is not straightforward
 3 since the involved phenomena occur in different regions of the fluidized bed. However, we
 4 have attempted to estimate key time scales by considering ideal compartments in the system,
 5 for which we have summarized results in Table 5. Most importantly, the calculated
 6 characteristic time for the droplet deposition is much smaller than the corresponding value for
 7 the spray evaporation. Thus, one might argue that droplets are quickly deposited, and hence
 8 only little evaporation can occur from air-suspended droplets. The predicted trend using CFD-
 9 DEM seems to be opposite, though: clearly, droplet evaporation is the dominating
 10 phenomenon. The trend seen in the CFD-DEM simulation can be explained by the fact that
 11 the droplets injected in the spray region can evaporate significantly during their downward
 12 movement. Hence, there are simply no droplets that can deposit on the particles surface left.
 13 We note in passing that the average time that droplet needs to collide with the particle bed
 14 before deposition is around 7.1×10^{-2} s (we have used the droplet injection speed, as well as
 15 the height difference $H_{inj-bed}$ between the injection region and the bed surface to estimate
 16 this time scale). This duration is much larger than characteristic time for the spray
 17 evaporation, i.e. 1.3×10^{-2} s. Thus, indeed, the droplets seem to have enough time to
 18 evaporate before they have a chance to meet particles moving in the system. It is now easy to
 19 identify a dimensionless “droplet-in-suspension” time $\tau_{d,susp}$ that governs whether droplet
 20 evaporation is relevant or not:

$$\tau_{d,susp} = \frac{H_{inj-bed}/u_{inj}}{t_{d,evap}} = \frac{H_{inj-bed} \rho_g}{u_{inj} \rho_d} \frac{4 D_{vap} \mu^{eq}}{d_d^2} \quad (21)$$

21 It should be noted that the evaporation time has been calculated based on the mass balance for
 22 vapour, and hence this characteristic time is independent from nozzle type and arrangement.
 23 In contrast, the droplet-in-suspension time is also a function of nozzle distance from the bed
 24 surface. Consequently, for nozzle arrangements different from the one studied here (e.g., a

1 bottom-spray configuration) the calculation of this time scale without detailed simulations is
2 not possible. This is because there is not defined distance between bed surface and the spray
3 region. The droplet-in-suspension time scale is indirectly affected by the nozzle type via the
4 droplet diameter and the droplet injection speed.

5 *Figure 5*

6 To summarize, it is of critical importance to consider the nozzle position relative to the bed,
7 and the speed of the injected droplets. Clearly, the spray should be located closer to the bed
8 surface, or the velocity of droplet injection should be increased, in case one aims on inducing
9 a fast deposition of droplets on the particle surface. Such a situation would be indicated by
10 $\tau_{d,susp} < 1$, i.e., the time droplets are suspended in air is smaller than a characteristic time for
11 their evaporation.

12 *Table 5*

13 Comparing the characteristic times for mass exchange between the particles and the fluid in
14 Table 5, droplet deposition occurs faster than the evaporation from the particle surface. Of
15 course, the rates have to match in a quasi-steady state, as reported in Table 4. The physical
16 meaning of the differences in the above time scales, that the dynamics of droplets deposition
17 are much faster, is a fact that has been already observed in connection with Figure 3a.

18 Aiming at investigating the effect of the studied phenomena on the bed performance in terms
19 of heat and mass exchange, the predicted mass loadings, temperatures, and LoD have been
20 plotted in Figures 4 and 5. As seen in Figure 4, in all cases in which the droplet evaporation is
21 considered, the gas temperature drops drastically within a few seconds. In contrast, the
22 particle temperature has the dynamic that differs significantly from that of the gas, and hence
23 the particle temperature decreases very slowly. This can be attributed to two facts: (i) the gas
24 is quickly cooled due to the high rate of evaporation in the spray region (which is located in

1 the top of the bed surface). Thus, the cooled gas leaves the bed without being in intense
2 contact with the particles. (ii) The mass (and hence the heat capacity) of gas in the system is
3 much smaller than that of the particles.

4 *Figure 6*

5 Another interesting observation is connected to the predicted temperature profiles along the
6 bed. As shown in Figure 5a, a sharp decrease of the gas temperature occurs near the top of the
7 bed. This temperature jump is absent in case evaporation from air-suspended droplets is not
8 considered (see Figure 5b). In the dense region (i.e., the bubbling bed), however, the gas
9 temperature is approximately constant though a marginal decrease near the bottom of the bed
10 (i.e., the gas inlet) was predicted for both cases (i.e., with or without evaporation from the
11 spray). Therefore, we conclude that the particle temperature is mainly governed by the
12 evaporation of liquid from the particle surface, and not by the evaporation from the air-
13 suspended droplets.

14 *Figure 7*

15 Comparison of the predicted LoD between Cases A and D reveals that spray evaporation
16 results in lower LoD. This is owing to the fact that a lower amount of liquid is available for
17 droplet deposition. However, in the case with no evaporation from the particle surface (i.e.,
18 Case C), the particle LoD increases approximately linearly over time. This is due to the fact
19 that the droplet evaporation rate is almost constant with rather insignificant fluctuations.
20 Consequently, an approximately constant amount of liquid is available for deposition on the
21 particles.

22 It should be noted that the predicted LoD is much smaller than its value in typical industrial
23 applications. This difference can be explained by the fact that the rate of evaporation from the
24 particle surface is over-predicted in this simulation: in industrial systems the liquid may be

1 trapped in the particles' pores, where the rate of evaporation is controlled by vapor diffusion.
2 In addition, in the present study, the droplet injection velocity is relatively low so that we can
3 observe the system in bubbling regime. Hence, the spray droplets spend more time
4 evaporating before interacting with the particles, so the deposition rate drops owing to the
5 reduction in the liquid mass loading. Finally, the fluidization gas has been considered
6 completely dry, while in physical systems the air is often humid.

7 A more detailed examination of the temperature profiles along the bed, as shown in Figure 5
8 manifests that the gas temperature is approximately constant along the dense bed for both
9 Cases A and D. However, the temperature dramatically decreases up to the spray zone center
10 for the case with droplet evaporation (see Figure 5a), followed by an increase with lower
11 slope due to a locally smaller droplet volume fraction. The latter results in a lower driving
12 force, and also mixing with the hot fluidization gas seems more intense in this region. It
13 should be mentioned that the predicted trend for the temperature and the mass loading in all
14 cases were similar except in Case D with no spray evaporation. As discerned from Figure 5,
15 at $x = 3.5 \text{ mm}$, which is off the center of the fluidized bed and hence outside of the spray
16 region, the gas temperature is higher. Also, the evaporation rate is lower in comparison to the
17 corresponding values at the center position (i.e. $x = 7 \text{ mm}$), even though the outlet gas
18 temperature is eventually the same at both lateral position. As depicted in Figure 5a, virtually
19 no spray loss was predicted, in contrast to the case without droplet evaporation (Figure 5b).

20 *Figure 8*

21 Another point discerned from Figure 5 is that the liquid and vapor mass loadings approach a
22 local maximum in the spray zone center in case with spray evaporation. Also, the liquid is
23 completely consumed near the bed surface due to the deposition and the evaporation in all
24 cases, as seen from the distribution of the droplet concentration and particles in Figures 6a
25 and 6c. As observed in this Figures 6a and 7, droplets are rapidly deposited on the particles

1 moving near the bed surface, and droplets are completely consumed in this region. The
2 droplets' penetration length is very short, especially for the case with spray evaporation, as
3 visible from the distribution of the particles' liquid content shown in Figure 9a (note that we
4 use a logarithmic scale in Figures 9-10, and that the ranges of the color-bars for panels a, b, c
5 in Figure 9 are different). This results in the formation of a region with high vapor content
6 near the top of the dense bed surface, as depicted in Figures 5 and 6b (for the latter see the
7 discussion in the next paragraph). Again, it appears that liquid evaporating from the particle
8 surface does not significantly affect the outlet vapor mass loading in most cases: the predicted
9 maps of liquid content shown in Figures 9a, 10a, and 10b indicate that this evaporation rate is
10 not a limiting factor. However, in case particles have initially a high wetness (see Figure 8d,
11 as well as Figure 9c), or the evaporation of air-suspended droplets is not considered (see
12 Figure 8b, as well as Figure 9b), evaporation from the particle surface plays a certain role.

13 *Figure 9*

14 To have a better understanding of phenomena taking place in the bed, contour-plots of source
15 terms for various cases and scalar quantities for Case A have been depicted in Figures 6-9 for
16 the bed cross section at $Y = 0$. Comparing the source terms in Figures 7a and 8a, droplets are
17 mainly consumed due to droplet evaporation, whereas the formation of vapour due to
18 evaporation from the particle surface is negligible. The predicted contour-plots for the vapour
19 mass loading and the bed voidage in Figures 6b-c also support this observation. It can be also
20 seen in Figure 6d that the temperature decreases significantly in the region limited between
21 the freeboard and the spray zone, which is associated to spray evaporation.

22 When neglecting droplet evaporation, i.e., in Case D (see Figures 7b and 8b), the liquid
23 droplets are consumed near the bed surface due to the deposition. The distribution of the
24 source term for vapour (Figure 8b) is now significantly different, and indicates a similarity to
25 the circular flow pattern of particles in the bubbling bed. In detail, the particles which manage

1 to reach the freeboard will filtrate the droplets out of the air. After the bubbles carrying these
2 particles burst, the particles will move laterally towards the wall, and then flow downward.
3 After reaching the bottom of the bed, these particles will be again carried upwards due to
4 bubble wake phenomena. This flow can form a circulation pattern for the solid movement in
5 the bed. During the movement of particles in such a way, their LoD gradually decreases due
6 to the evaporation induced by the contact with the hot dry gas entering the fluidized bed.

7 The Effect of the Surface Coverage Model

8 The rate of evaporation from particles plays an important role when computing the LoD, and
9 this rate is highly dependent on the area available for the evaporation on the particle surface.
10 Therefore, two surface coverage models were implemented in the CFDEM® code, and their
11 effects were examined. Furthermore, the effects of initial particle liquid content on the
12 equilibrium LoD and the associated exchange rates were evaluated. In detail, the initial LoD
13 was set to the value close to i) the equilibrium value of LoD calculated based on the droplet
14 mass loading in the injection zone, (obtained as a function of injection rate, gas flow rate, and
15 injection zone volume) i.e. $LoD = 3.6 \times 10^{-4}$; ii) the particle-averaged equilibrium value of
16 LoD calculated based on a domain-averaged deposition rate and the number of particles in the
17 bed, i.e. $LoD = 2.49 \times 10^{-7}$; and iii) the value of LoD calculated based on a given surface
18 coverage of 0.5, i.e. $LoD = 0.395$. More details about the calculation of the initial LoD for
19 each case can be found in Appendix C.

20 *Figure 10*

21 The results of the above described simulations have been depicted in Figures 11-13
22 respectively. As discerned from these figures, for a specific surface coverage model, i.e., the
23 linear model (right panel) or Kariuki's model (left panel), a higher initial LoD results in a
24 higher rate of droplet deposition. This is due to the fact that higher initial LoD causes larger
25 evaporation rates from the particle surface, such that the driving force for spray droplet

1 evaporation is suppressed. This results in higher droplet mass loading of the air, and
2 consequently a higher deposition rate. In contrast, and as depicted in Figures 14 and 15, the
3 predicted quasi steady state LoD is approximately in the same order of magnitude and is
4 within 25.4% of our results for the base case, i.e., Case A upon using Kariuki's model, for
5 different initial LoDs but identical injection rates.

6 Comparing the deposition rate for the case with different initial LoDs in Figures 11-13, it can
7 be concluded that for an initially higher LoD, the particle evaporation rate exceeds the droplet
8 deposition rate due to the larger wet surface area in the fluidized bed. In this case, the droplet
9 deposition occurs only near the free interface and is limited by the injection rate of droplets.
10 Besides, decreasing the driving force, the evaporation from particle surface discourages spray
11 evaporation, which makes liquid more available for the droplet deposition.

12 *Figure 11*

13 In case of using a very high value for the initial LoD, as shown in Figure 13a, the highest rate
14 for the evaporation from the particles was predicted. This is because of the larger surface
15 coverage and smaller characteristic time (see Table 5: the time scale for evaporating liquid on
16 the particle surface is inversely proportional to the surface coverage). In the case of strong
17 evaporation from the particle surface the rate of the droplet evaporation, as depicted in Figure
18 7d, is suppressed. This is due to the low gas temperature, and saturated air stemming from the
19 evaporation from the particle surface. In this case, and when considering Figure 16a, the
20 predicted mean particle temperature and the outlet gas temperature decrease with almost the
21 same rate. This is due to the mixing of cool particles with the hot gas in the dense bed. Also, it
22 can be observed that the gas temperature fluctuates marginally due to the fluidized bed nature
23 in this case. In addition, considerably high initial LoDs leads to higher liquid mass loading,
24 and a high rate of evaporation from the particle surface in the bed, as shown in Figure 8d.
25 Consequently, a large amount of water vapor is released in the system. Also, for this situation,

1 the condensation of water vapor near the bed surface was predicted. This means that, in this
2 region, the rate of evaporation from particles is so high that vapor mass loading can exceed
3 the corresponding saturation value in the gas phase. Consequently the driving force for the
4 droplet evaporation will be reversed. It should be mentioned that the relative velocity
5 between the gas and the solid enjoys the highest values near the bed surface. Hence, the mass
6 transfer coefficient, and accordingly the evaporation rate are highest near the bed surface.

7 Also, it should be noted that a very slow decrease in the LoD was predicted in the case with
8 highest initial LoD, as depicted in Figures 16a-b. Thus, a significantly larger simulation time
9 would be required to understand the full dynamics of the drying process. An appropriate
10 approach to overcome the high computational cost is to use simple 1D or 0D model to capture
11 phenomena with such a long time scale. Unfortunately, such a modeling approach was not in
12 the focus of the present contribution, but can be followed in future work. Specifically, one could
13 simplify the expressions presented in our mathematical model for mass and heat transfer, as well
14 as derive a transport equation for the liquid deposited on the particles. Such transport equations
15 would have to include a term accounting for transport due to dispersion by unresolved fluid or
16 particle motion in case a 1D approach is chosen. Also, a 1D or 0D approach would require more
17 advanced closures for average heat and mass transfer coefficients since these coefficients are
18 significantly altered by bubbling, and cannot be set equal to the local transfer coefficients used in
19 the present work. Thus, while the development of simplified models might appear straight
20 forward on a first view, there are significant hurdles connected to the closures used in future 1D or
21 0D models.

22 *Figure 12*

23 One important point discerned from Figures 13b, and 16b is that due to no evaporation from
24 the particle surface at liquid contents smaller than the critical value, the particle LoD increases
25 linearly over the time. Also, the particle temperature decreases very slowly due to the heat

1 exchange with the gas phase. Consequently, the critical value for LoD at which the
2 evaporation starts seems to be crucial to predicting the behavior of the bed. This will come to
3 play upon studying porous particles. Therefore, in the case of using a linear model (for
4 modeling surface coverage), and when assuming a high value for $L_{p,no\ evap}^*$, the bed behaves
5 in a distinctly different way. As a result, another simulation was performed using critical LoD
6 of zero to compare the bed performance between two surface coverage models in a more
7 straight forward way.

8 *Table 6*

9 Comparing the different surface coverage models, as discerned from Figures 11 to 12 and
10 Figures 14 to 15, the characteristic time for the evaporation from the particle surface for
11 Kariuki's model is shorter than the corresponding time for the linear model. This is based on
12 data for the slope of LoD against time presented in Table 6. This demonstrates that LoD in
13 Kariuki's model reaches a pseudo steady state condition in a shorter time. It should be noted
14 that the slope at different initial LoDs for Kariuki's model is identical. In addition, as
15 computed in Table 7, the linear model over-predicts the quasi steady-state LoD by a
16 maximum of 86.9 % in comparison to Kariuki's Model. However, the predicted gas and
17 particle temperatures are similar for both models (i.e., they are within 1.33×10^{-2} %
18 difference). Therefore, using different models for the surface coverage results in a variation
19 of the predicted LoD by a factor of approximately two. In contrast, the predicted gas and
20 particle temperatures are only insignificantly affected by the surface coverage model in the
21 studied cases. Again, this is due to the dominance of the droplet evaporation rate over the
22 corresponding rate of evaporation from the particle surface at low particle liquid contents.

23 *Figure 13*

24 It can be concluded that the implementation of suitable surface coverage model is of key
25 importance for the correct prediction of the competition between evaporation from the spray

1 and from the particle surface. This is due to their contribution in the amount and position of
2 vapor formation in the bed. This can influence the competition between spray evaporation and
3 droplet deposition. This claim can be proven by considering the exchange rates shown in
4 Figure 13a with high initial surface coverage. Moreover, upon assuming the formation of a
5 continuous film on the particle surface, i.e., $\psi_{liq} = 1.0$, the characteristic time for particle
6 evaporation is 2-3 orders of magnitude larger than the corresponding times for the deposition
7 and spray evaporation, see the data in Table 5. These competitions among exchange rates also
8 play a key role in the computation of gas moisture and humidity. What is more, adopting
9 appropriate surface coverage model is vital in accurate computation of LoD, and consequently
10 the liquid available for liquid bridge formation between wet particles. Those liquid bridges are
11 essential for granulation process, since they induce granule growth and stabilize existing
12 granules. In detail, the results of the simulations in this study proved that simplified model,
13 i.e., a linear model can overestimate the particle liquid content in comparison with the more
14 realistic model such as Kariuki's model. The latter has been developed based on Bernoulli's
15 trials, and an assumed uniformly random distribution of droplets on the particle surface. In
16 addition, this model has been validated with experimental data. In short, the choice of the
17 surface coverage model is very important for the drying and granulation processes, at least for
18 the case of non-porous particles.

Table 7

19 **Effect of Operation Conditions**

20 The Effect of the Injection Rate

21 Aiming at comparing the dependency of exchange rates on liquid mass loading, the effect of
22 the droplet injection rate was investigated. The results of these simulations have been
23 presented in Figure 17, in which the injection rate ratio is simply the used liquid injection rate
24 divided by the rate used in the base case (see Table 2). It can be readily discerned from Figure

1 17a that an increase in the injection rate reduces the (relative) spray evaporation contribution.
2 This finding proves that when increasing the injection rate, the fluid flowing in the spray
3 region will be saturated with vapor and consequently higher amount of droplets will be
4 available for deposition on the particles. The predicted spray loss also proves this saturation
5 condition when comparing the sums of the normalized exchange rates shown in Figure 17a.

6 *Figure 14*

7 For the injection rate ratios higher than three, the spray evaporation rate ratio decreases almost
8 linearly with the injection rate ratio. This proves that the rate of evaporation will remain
9 approximately constant and will not change with the injection rate. Also, the trend of the
10 predicted (outlet) gas temperature shown in Figure 17b demonstrates this claim. As seen in
11 this figure, the gas temperature drops significantly for higher injection rates, and then remains
12 constant for injection rate ratios higher than 6. For these very high injection rates, a more
13 intense droplet deposition is observed. Thus, the deposition rate is dependent on the liquid
14 mass loading to a large extent. Since evaporation from particles is in balance with the
15 deposition rate at quasi steady state conditions, the same trend can be observed for the
16 evaporation rate from the particle surface. Therefore, the particle temperature will decrease
17 with increasing liquid injection rates, while the LoD will increase as seen in Figure 17b.

18 *Figure 15*

19 The Effect of the Inlet Temperature

20 Since operating temperature may strongly impact the evaporation in the wet fluidized bed, the
21 effect of inlet temperature was investigated as well. As discerned from Figure 18a, an increase
22 in the inlet temperature decreases the deposition rate and consequently the evaporation rate
23 from the particle surface. This means that the (dimensionless) rate of spray evaporation will
24 gradually approach unity when increasing the gas inlet temperature. Such an increase can be
25 explained considering the fact that the rise in temperature provides the droplets with larger

1 driving force because of higher saturation pressure. Therefore, a lower amount of droplets
2 have the chance to collide the bed surface, and meet the particles for deposition. As a result,
3 the particle LoD will drop with the same trend as the deposition rate. On the other hand, the
4 particle and the (outlet) gas temperature will linearly increase with the inlet gas temperature.
5 This is simply to explain based on the fact of a constant injection rate, and the overall heat
6 balance of the system.

7 **Comparison of 2D and 3D simulation**

8 Since the computational cost for real 3D case is not affordable, the developed models were
9 studied in a pseudo 2D fluidized bed so far. In order to evaluate the application of developed
10 model in a 3D bed, a simulation was performed for the bed filled with one million particles. In
11 the 3D simulation, the same ratio of the liquid injection rate and the mass of particles was
12 used. In the 3D simulation, the injection region was positioned in the centre of the domain
13 (see Figure 1 and Table 2).

14 *Figure 16*

15 As plotted in Figures 19a-b, the predicted deposition rate is higher in the 3D case, since the
16 injection region is more concentrated, which means the ratio of the projected area of injection
17 and the bed's cross sectional is smaller. Hence, the local cooling of the gas is more intense,
18 and a smaller amount of liquid evaporates above the particle bed. Consequently, a larger
19 fraction of the surface of the bed is exposed to droplets, causing higher deposition rates. It can
20 be also discerned form Figures 10a-b that the particles moving on the bed surface below the
21 spray region receive more droplets on their surface. Moreover, as shown in Figure 10c,
22 bubbles mainly move in the central region of the bed. The particles dragged in the bubble
23 wake have somewhat higher velocities after bubble bursting in the freeboard, since the speed
24 of a bubble is in the order of 0.2 [m/s]. Hence, the rate of droplet deposition, and consequently
25 their LoD will be higher for these particles. This effect is followed by a higher LoD predicted

1 in the 3D simulations as shown in Figures 19c-d. However, the predicted outlet temperature is
2 identical in both cases.

3 *Figure 17*

4 **Conclusion**

5 The exchange of mass and heat between gas, particle, and droplet was simultaneously
6 simulated in a wet fluidized bed using a full-physics CFD-DEM approach. In detail, sub-
7 models in the CFDEM® code were developed that consider i) droplet deposition on particles,
8 ii) evaporation of freely-flowing droplets, and iii) evaporation of deposited droplets from
9 particle surface. After successful implementation and verification of these models, the code
10 was used for the simulation of a bubbling fluidized bed with liquid injection. Particularly, the
11 contributions of the involved phenomena in the bed performance were evaluated. Also, we
12 included the cooling effect due to evaporation: this closes an important gap, namely the back-
13 coupling of evaporative cooling on the local evaporation rate of liquid in a wet fluidized bed.
14 Most important, our simulations indicate that while the particle temperature is almost
15 homogeneous, the gas temperature fluctuates significantly in the freeboard of the fluidized
16 bed. The results of our simulations indicated that the rate of evaporation from the spray is two
17 orders of magnitude higher than the rates of the evaporation from the particle surface and the
18 droplet deposition. This is due to the fact that the “droplet-in-suspension” time scale is larger
19 than a typical droplet evaporation time. The ratio of these time scales is indirectly affected by
20 the nozzle type via the droplet diameter and the droplet injection speed. The droplet diameter
21 is relatively small in this study due to industry demand, resulting in fast droplet evaporation.
22 However, droplet size can be easily adjusted if necessary for different applications to define a
23 suitable dimensionless “droplet-in-suspension” time. Also, the relative importance of all
24 relevant exchange rates was analysed through comparison of the characteristic time scales for
25 each phenomenon, i.e., droplet deposition, as well as evaporation from spray and particle

1 surface. While the interpretation of these time scales is non-trivial, they may guide
2 practitioners and modeling experts upon developing compartment models. Most important,
3 we have identified a dimensionless parameter that helps to decide when evaporation from the
4 droplets should be taken into account or not.

5 *Figure 18*

6 Moreover, it was demonstrated that the gas and particle temperatures are mainly influenced
7 by the rates of evaporation from the droplets and the particle surface, respectively. In the case
8 of no droplet evaporation, due to the efficient particle mixing in the bed, similar temperatures
9 were predicted for both phases. In this case, the particle LoD increases 2 orders of magnitude,
10 showing that the LoD is highly sensitive to the predicted evaporation from air-suspended
11 droplets.

12 *Figure 19*

13 Furthermore, the effect of surface coverage models was investigated, and a strong influence
14 on the particle LoD was proved. Therefore, implementation of a suitable surface coverage
15 model is crucial when attempting to accurately calculate the particles' LoD, as well as the gas
16 moisture and humidity. This clearly motivates more studies in the area of surface coverage
17 models, and clearly stresses the importance of the work done by Kariuki et al.²⁸ Apart from
18 this, the effect of injection rate and inlet gas temperature was investigated. Since the particle
19 bed has a fairly uniform temperature, we speculate that it will be easy to calibrate
20 compartment models with the knowledge gained in the present study. Also, future work may
21 develop such a compartment model, and lead to an immediate industrial application that
22 allows a prediction of the long-term evolution of the bed dynamics.

23 In summary, the developed code and understanding may be useful for future studies of
24 granulation processes – both incorporating porous and non-porous particles. However, some

1 extensions that allow full-physics simulations of the latter seem necessary. For example, this
2 could include models for intra-particle transport processes, e.g., of water vapour within the
3 pores. In addition, the future development of appropriate surface coverage model that account
4 for the particles' porosity will be essential. In addition, the newly defined time scale for
5 evaporation from the droplets could help to improve the previous work of Sutkar et al. ¹³.
6 Finally, the model of Kolakaluri ²⁹ is of central importance. Clearly, more work in the
7 direction of filtration models for poly-disperse systems would be helpful to improve the
8 fidelity of future full-physics granulation CFD-DEM models.

9

1 Notation

Latin Letters

a_d	$1/m$	specific mass transfer surface area of droplet, $6/d_d$
a_{dp}	$1/m$	specific surface area of particle available for droplet evaporation
a_p	$1/m$	Particle specific surface area, $(1 - \phi_f) 6/d_p$
C_p	$m^2 kg/s^2/K$	Thermal capacity
d_d	m	Droplet diameter
D_{eff}	m^2/s	Effective diffusivity of vapor in air
D_{vap}	m^2/s	Molecular diffusivity of vapor in air
d_p	m	Particle Diameter
e	–	Restitution coefficient
f	m^2/m^2	fraction of particle surface coated by droplet
$f_{cont,i}$	N	Contact force exerted on i^{th} particle
H_{bed}	M	Bed height in y direction
H_{inj}	M	Injection zone height in y direction
g	m/s^2	gravity
h	$kg/s^3/K$	Heat transfer coefficient
$I_{p,i}$	$kg m^2$	particles moment of inertia
L_{bed}	M	Bed length in x direction
L_{inj}	m	Injection zone length in x direction
L_p^*	m^3/m^3	volume fraction of liquid on particle

$L_{p,noevap}^*$	m^3/m^3	volume fraction of liquid on particle at which evaporation from particle can start
LoD	–	Loss on drying, defined as mass fraction of liquid in the particle
N_p	–	Number of particle in the system
Nu	–	Nusselt Number, hd_p/λ_f
P_f	Pa	Pressure
Pr	–	Prandtl Number, $C_p\nu_f\rho_f/\lambda_f$
Re	–	Reynolds number
\dot{S}_d	$kg/s/m^3$	Rate of droplet deposition on particle
$\dot{S}_{evap,p}$	$kg/s/m^3$	Rate of evaporation from particle surface
$\dot{S}_{evap,f}$	$kg/s/m^3$	Rate of evaporation from spray
\dot{S}_{inj}	$kg/s/m^3$	Rate of liquid (droplet) injection
Sh	–	Sherwood number, $\beta d_p/D_{vap}$
St	–	Droplet Stokes Number
St_{eff}^*	–	Effective droplet Stokes Number
T	K	Temperature
t	s	Time
t_{sim}	s	Simulation time
\mathbf{u}_d	m/s	droplet velocity, $\mathbf{u}_d = \mathbf{u}_f$
\mathbf{u}_f	m/s	Fluid velocity
V_{inj}	m^3	Injection zone volume

V_p	m^3	Particle volume
w_{bed}	m	Bed width in y direction
w_{inj}	m	Injection zone width in y direction
Y	m	Distance from the origin in y direction
Z_{inj}	m	Injection zone width in y direction
Greek Letter		
β	m/s	Mass transfer coefficient
β_{sf}	$kg/m^3/s$	Solid-fluid momentum exchange coefficient
ΔH_{evap}	J/kg	Heat of evaporation
Δt_{CFD}	s	Time step for CFD
Δt_{DEM}	s	Time step for DEM
η_n	kg/s	Normal viscous damping coefficient
η_s	–	Single collector efficiency
η_t	kg/s	Tangential viscous damping coefficient
k_n	kg/s^2	Normal spring stiffness
k_t	kg/s^2	tangential spring stiffness
λ	$1/m$	Filtration coefficient
λ_{eff}	$m\ kg/s^3/K$	Effective Thermal conductivity
μ_c	–	Coulomb friction coefficient
μ_{liq}	kg/kg	Mass loading of liquid water in gas phase

μ_{vap}	kg/kg	Mass loading of water vapor in gas phase
ν_f	m^2/s	Kinematic viscosity
ρ_f	kg/m^3	Fluid density
$\rho_{w,sat}$	kg/m^3	Saturation density of water vapor
τ_f	Pa	fluid stress tensor
$\tau_{d,susp}$	–	Dimensionless “droplet-in-suspension” time scale
ϕ_j	–	volume fraction of phase j
Φ_d	N/m^3	Force exerted by particles on fluid phase per unit volume of cell.
Φ_p	–	particle coating number
ψ_{liq}	m^2/m^2	Particle surface coverage
$\omega_{p,i}$	rad/s	Particle angular velocity

subscripts

d	droplet
f	Fluid
i	i^{th} particle
P	Particle
liq	Liquid (water)
vap	vapor (water)

1
2
3
4
5
6
7
8

Literature Cited

1. Mörl L, Heinrich S, Peglow M. Fluidized bed spray granulation. *Handbook of powder technology*. 2007;11:21-188.
2. Maronga S, Wnukowski P. The use of humidity and temperature profiles in optimizing the size of fluidized bed in a coating process. *Chemical Engineering and Processing: Process Intensification*. 1998;37(5):423-432.
3. Sherony DF. A model of surface renewal with application to fluid bed coating of particles. *Chemical engineering science*. 1981;36(5):845-848.

- 1 4. Li J, Freireich B, Wassgren C, Litster JD. A general compartment-based population balance model
2 for particle coating and layered granulation. *AIChE Journal*. 2012;58(5):1397-1408.
- 3 5. Börner M, Peglow M, Tsotsas E. Derivation of parameters for a two compartment population
4 balance model of Wurster fluidised bed granulation. *Powder technology*. 2013;238:122-131.
- 5 6. Rajniak P, Stepanek F, Dhanasekharan K, Fan R, Mancinelli C, Chern R. A combined experimental
6 and computational study of wet granulation in a Wurster fluid bed granulator. *Powder
7 Technology*. 2009;189(2):190-201.
- 8 7. Tan H, Goldschmidt M, Boerefijn R, Hounslow M, Salman A, Kuipers J. Building population balance
9 model for fluidized bed melt granulation: lessons from kinetic theory of granular flow. *Powder
10 Technology*. 2004;142(2):103-109.
- 11 8. Vreman A, Van Lare C, Hounslow M. A basic population balance model for fluid bed spray
12 granulation. *Chemical Engineering Science*. 2009;64(21):4389-4398.
- 13 9. Heinrich S, Peglow M, Ihlow M, Henneberg M, Mörl L. Analysis of the start-up process in
14 continuous fluidized bed spray granulation by population balance modelling. *Chemical
15 Engineering Science*. 2002;57(20):4369-4390.
- 16 10. Link J, Godlieb W, Deen N, Kuipers J. Discrete element study of granulation in a spout-fluidized
17 bed. *Chemical Engineering Science*. 2007;62(1):195-207.
- 18 11. Fries L, Antonyuk S, Heinrich S, Palzer S. DEM-CFD modeling of a fluidized bed spray granulator.
19 *Chemical Engineering Science*. 2011;66(11):2340-2355.
- 20 12. Börner M, Hagemeier T, Ganzer G, Peglow M, Tsotsas E. Experimental spray zone characterization
21 in top-spray fluidized bed granulation. *Chemical Engineering Science*. 2014;116:317-330.
- 22 13. Sutkar VS, Deen NG, Patil AV, et al. CFD-DEM model for coupled heat and mass transfer in a spout
23 fluidized bed with liquid injection. *Chemical Engineering Journal*. 2016;288:185-197.
- 24 14. Štěpánek F, Rajniak P. Droplet morphologies on particles with macroscopic surface roughness.
25 *Langmuir*. 2006;22(3):917-923.
- 26 15. McDougall S, Saberian M, Briens C, Berruti F, Chan E. Using dynamic pressure signals to assess the
27 effects of injected liquid on fluidized bed properties. *Chemical Engineering and Processing: Process
28 Intensification*. 2005;44(7):701-708.
- 29 16. Ariyapadi S, Holdsworth DW, Norley CJ, Berruti F, Briens C. Digital X-ray imaging technique to
30 study the horizontal injection of gas-liquid jets into fluidized beds. *International Journal of
31 Chemical Reactor Engineering*. 2003;1(1).
- 32 17. Briens C, Dawe M, Berruti F. Effect of a draft tube on gas-liquid jet boundaries in a gas-solid
33 fluidized bed. *Chemical Engineering and Processing: Process Intensification*. 2009;48(4):871-877.
- 34 18. Zhu H, Zhou Z, Yang R, Yu A. Discrete particle simulation of particulate systems: theoretical
35 developments. *Chemical Engineering Science*. 2007;62(13):3378-3396.
- 36 19. Radl S, Kalvoda E, Glasser BJ, Khinast JG. Mixing characteristics of wet granular matter in a bladed
37 mixer. *Powder Technology*. 2010;200(3):171-189.
- 38 20. Girardi M, Radl S, Sundaresan S. Simulating wet gas-solid fluidized beds using coarse-grid CFD-
39 DEM. *Chemical Engineering Science*. 2016;144:224-238.
- 40 21. Van Buijtenen MS, Deen NG, Heinrich S, Antonyuk S, Kuipers J. A discrete element study of wet
41 particle-particle interaction during granulation in a spout fluidized bed. *The Canadian Journal of
42 Chemical Engineering*. 2009;87(2):308-317.
- 43 22. Kloss C, Goniva C, Hager A, Amberger S, Pirker S. Models, algorithms and validation for
44 opensource DEM and CFD-DEM. *Progress in Computational Fluid Dynamics, an International
45 Journal*. 2012;12(2-3):140-152.
- 46 23. Kloss C, Goniva C. LIGGGHTS-open source discrete element simulations of granular materials
47 based on LAMMPS. *Supplemental Proceedings: Materials Fabrication, Properties, Characterization,
48 and Modeling, Volume 2*. 2011:781-788.
- 49 24. Jasak H, Jemcov A, Tukovic Z. OpenFOAM: A C++ library for complex physics simulations. Paper
50 presented at: International workshop on coupled methods in numerical dynamics2007.
- 51 25. Beetstra R, Van der Hoef M, Kuipers J. Drag force of intermediate Reynolds number flow past
52 mono-and bidisperse arrays of spheres. *AIChE Journal*. 2007;53(2):489-501.
- 53 26. Kloss C. LIGGGHTS-PUBLIC Documentation, Version 3.X.
- 54 27. Deen NG, Kriebitzsch SH, van der Hoef MA, Kuipers J. Direct numerical simulation of flow and heat
55 transfer in dense fluid-particle systems. *Chemical Engineering Science*. 2012;81:329-344.
- 56 28. Kariuki WI, Freireich B, Smith RM, Rhodes M, Hapgood KP. Distribution nucleation: quantifying
57 liquid distribution on the particle surface using the dimensionless particle coating number.
58 *Chemical Engineering Science*. 2013;92:134-145.
- 59 29. Kolakaluri R. *Direct Numerical Simulations and Analytical Modeling of Granular Filtration*, Iowa
60 State University 2013.

Appendix A: Model Verification

In order to be assured of the correct implementation of the implemented models, several verification studies were performed. Clearly, such verification studies cannot substitute a thorough validation against experimental results. However, the results presented below document the correct functionality of our models in a number of relevant (but synthetic) flow situations.

A.1. Droplet Deposition on Particle

In order to examine the accuracy of model implementation, assuming an instantaneous interaction between droplets and the particle bed (i.e., the granules), a sink term can be defined in the transport equation for the droplet concentration as follows:

$$\frac{\partial(\mu_{liq}\varphi_f\rho_f)}{\partial t} + \nabla \cdot (u_f\mu_{liq}\varphi_f\rho_f) = \dot{S}_d \quad (\text{A1})$$

Aimed at model verification, an analytical solution was obtained for a packed bed with a clean-bed filter (filtration coefficient is assumed to be constant along the bed) as

$$\ln\left(\frac{\mu_{liq}}{\mu_{liq,0}}\right) = -\lambda x \quad (\text{A2})$$

Where the filtration coefficient λ is calculated based on volume-averaged voidage and fluid velocity in the packed bed.

The results of CFD-DEM simulation and analytical solution for droplet mass loading along the bed was presented in Figure A.1. As seen in this figure, the predicted non-dimensional droplet mass loading is in good agreement with analytical solution at the positions where voidage is constant. However, small deviation can be observed near the bed inlet and bed surface, which can be attributed to the porosity distribution. In detail, void fraction averaging method results in higher gas volume fraction in the first and last rows of cell in the dense bed.

1 Since filtration coefficient strongly depends on particle volume fraction, small deviation is
2 expected in these regions

3

4 *Figure A.1.*

5 **A.2. Droplet Evaporation from the Particle Surface**

6 A.2.1. Deposited Droplet Evaporation in Flowing Fluid

7 Aimed at verifying the implemented model for heat exchange between particles and fluid
8 phase, initially heat balance equation for both gas and particle phase for 1D packed bed was
9 derived as

$$\varphi_f \rho_f C_{p,g} \frac{\partial T_g}{\partial t} = -\varphi_f \rho_f C_{p,g} u_g \frac{\partial T_g}{\partial z} - h a (T_g - T_p) \quad (A3)$$

$$(1 - \varphi_f) \rho_p C_{p,p} \frac{\partial T_p}{\partial t} = h a (T_g - T_p) - \dot{q}_{evap} \quad (A4)$$

10

11 T_g and T_p were theoretically calculated. For verification of model, a pseudo 2D packed bed
12 was simulated in CFDEM. The simulation condition was presented in Table A.1. It should be
13 mentioned that particles were fixed in the DEM simulation so that the bed voidage and
14 relative velocity between gas and particle can remain constant during simulation time.

15 *Table A.1.*

16 The results of model verification were depicted in Figure A.2. The temperatures predicted
17 through CFD-DEM simulation is in excellent agreement with corresponding analytical values
18 at different heights.

19 *Figure A.2.*

1 A.2.1. Deposited Droplet Evaporation in Stagnant Fluid

2 For verification of implemented model for evaporation from particle surface in particle side, a
3 simulation was performed for a bed of particle without gas flow. To do so, particle-fluid heat
4 exchange was not considered. The rate of evaporation was assumed constant in this case. As
5 depicted in Figure A.3, mean particle liquid content and particle temperature as well as vapor
6 mass loading over time were in excellent agreement with the analytical solution

7 *Figure A.3*

8 **A.3. Spray Evaporation**

9 In order to verify the implemented model for spray evaporation, the mass transport equation
10 for vapor mass loading was numerically solved

$$\frac{\partial \mu_{vap} \varphi_f \rho_f}{\partial t} + \nabla \cdot (u_f \mu_{vap} \varphi_f \rho_f) = \dot{S}_{evap} \quad (A5)$$

11

12 The droplet was injected in the bed inlet. For simplification, the characteristic time for droplet
13 evaporation was assumed constant. Besides, the liquid mass loading is high enough to have a
14 constant surface area for evaporation. As shown in Figure A.4, the predicted vapor mass
15 loading is in good agreement with corresponding analytical values at various heights.

16 *Figure A.4*

17

18 **Appendix B: Characteristic Time Scales**

19 The average characteristic times for various phenomena taking place in the fluid bed
20 granulator are calculated to compare the relative importance of these phenomena.

21 B.1 Spray Evaporation (Saturation Time Scale)

22 The mass balance equation for water vapour in a fixed volume can be derived as:

$$\partial_t m_{vap} = A_d \beta_d (\rho^{eq} - \rho_v), \quad (B1)$$

1 where ∂_t denotes the time derivative, and

$$A_d = V_{tot} a_d = V_{tot} \varphi_d \frac{6}{d_d} \quad (B2)$$

$$\rho^{eq} = \mu^{eq} \rho_g \quad (B3)$$

$$\rho_v = \mu_v \rho_g \quad (B4)$$

2 If we assume that droplet volume fraction, i.e. φ_d is small, the variation of total volume, V_{tot} ,
3 is marginal, such that the Equation B1 can be rewritten as an equation in which all terms are

4 $O(1)$:

$$V_{tot} \rho_g \partial_t \mu_v = V_{tot} \varphi_d \frac{6}{d_d} \beta_d \rho_g (\mu^{eq} - \mu_v) \quad (B5)$$

$$\frac{d_d}{6 \beta_d \varphi_d} \partial_t \frac{\mu_v}{\mu^{eq}} = t_{v, evap} \partial_t \frac{\mu_v}{\mu^{eq}} = 1 - \frac{\mu_v}{\mu^{eq}} \quad (B6)$$

5 For zero-slip velocity, the Sherwood number equals 2, such that the mass transfer coefficient
6 is given by

$$\beta = \frac{Sh D_{vapor}}{d_d} = \frac{2 D_{vapor}}{d_d} \quad (B7)$$

7 Droplet volume fraction can be calculated as

$$\varphi_d = \frac{V_d}{V_{tot}} = \frac{m_d / \rho_d}{m_d / \rho_d + m_g / \rho_g} = \frac{\rho_g / \rho_d \mu_d}{\rho_g / \rho_d \mu_d + 1} \cong \rho_g / \rho_d \mu_d \quad (B8)$$

8 Therefore, droplet evaporation characteristic time is:

$$t_{v,evap} = \frac{d_d^2}{12 D_{vapor} \rho_g / \rho_d \mu_d} \quad (\text{B9})$$

1 B.2 Spray Evaporation (Droplet Evaporation Time Scale)

2 The mass balance equation for a single droplet can be derived as

$$\partial_t m_d = A_d \beta_d (\rho^{eq} - \rho_v) \quad (\text{B10})$$

3 Inserting the definition of droplet mass, surface area, and mass transfer coefficient yields

4 again an equation in which all terms are O(1):

$$\partial_t \left(\rho_d \frac{\pi}{6} d_d^3 \right) = \pi d_d^2 \frac{2 D_{vapor}}{d_d} \rho_g (\mu^{eq} - \mu_v) \quad (\text{B11})$$

$$\frac{\rho_d}{\rho_g} \frac{d_d^2}{4 D_{vapor} \mu^{eq}} \partial_t d_d^* = t_{d,evap} \partial_t d_d^* = 1 - \frac{\mu_v}{\mu^{eq}} \quad (\text{B12})$$

5 Here the asterisk refers to a dimensionless quantity, i.e., the droplet diameter. Thus, we arrive

6 at:

$$t_{d,evap} = \frac{\rho_d}{\rho_g} \frac{d_d^2}{4 D_{vapor} \mu^{eq}} \quad (\text{B13})$$

7 B.3 Evaporation from Particle Surface

8 The mass balance equation for water vapour upon evaporation from particle can be written as

$$\partial_t m_{vap} = A_d \psi_{liq} \beta_p (\rho^{eq} - \rho_v) \quad (\text{B14})$$

$$(1 - \varphi_p) V_{tot} \rho_g \partial_t \mu_v = V_{tot} \varphi_p \frac{6}{d_p} \beta_p \rho_g \psi_{liq} (\mu^{eq} - \mu_v) \quad (\text{B15})$$

$$\frac{1 - \varphi_p}{\varphi_p} \frac{d_p}{6 \beta_p \psi_{liq}} \partial_t \frac{\mu_v}{\mu^{eq}} = t_{evap,p} \partial_t \frac{\mu_v}{\mu^{eq}} = 1 - \frac{\mu_v}{\mu^{eq}} \quad (\text{B16})$$

1 Considering the same methodology as above, the characteristic time for evaporation from the
 2 particle surface can be expressed as

$$t_{evap,p} = \frac{1 - \varphi_p}{\varphi_p} \frac{d_p^2}{6 Sh D_{vapor} \psi_{liq}} \quad (B17)$$

3 In which the Sherwood Number must be calculated using the correlation presented by Deen
 4 et al. since mass transfer occurs from a dense gas-particle suspension:

$$Sh = (7 - 10\varphi_f + 5\varphi_f^2)(1 + 0.7Re^{0.2}Pr^{1/3}) + (1.33 - 2.4\varphi_f + 1.2\varphi_f^2)Re^{0.7}Pr^{1/3} \quad (B18)$$

5 Re is taken as that at the minimum fluidization velocity, same as the value for the voidage.

6 B.4 Droplet Deposition

7 The characteristic time for deposition of droplet can be calculated following Kolakaluri:

$$t_{depos} = \frac{1}{\lambda |u_f - u_p|} \quad (B19)$$

8

9 **Appendix C: Calculation of Equilibrium Surface Coverage**

10 In order to examine the effect of different initial particle wetness levels on the exchange rates
 11 and bed behavior, three different scenarios as described below were investigated.

12 **C.1. LoD based on the Droplet Mass Loading in the Injection Zone**

13 We assumed that $\rho_v \approx 0$, a quasi-steady state, and that the particles experience the droplet
 14 mass loading given by the injected droplet mass, the induced air velocity (u_{inj}), and a typical
 15 cross-sectional area of injection A_{inj} :

$$\frac{d(m_{lp})}{dt} = 0 = \dot{m}_{dep} - \dot{m}_{evap} \quad (C1)$$

$$\dot{m}_{evap} = A_p \psi_{liq} \beta_p \rho^{eq} \quad (C2)$$

$$\dot{m}_{dep} = \lambda |u_f - u_p| \mu_{liq} \rho_f \frac{\phi_f}{1 - \phi_f} V_p \quad (C3)$$

$$\psi_{liq} = \frac{\lambda |u_{inj} - u_p| \frac{\dot{m}_{inj}}{u_{inj} A_{inj}} \frac{\phi_f}{1 - \phi_f} \frac{d_p^2}{6}}{D_{vap} sh \rho^{eq}} \quad (C4)$$

1

2 Since the rate of deposition is calculated based on the droplet concentration in the spray zone,
 3 the corresponding L_p^* represents the maximum expected liquid content of particles. By using
 4 Kariuki's surface coverage model (see Section C.4 below) we can now estimate the initial
 5 surface coverage, and consequently the initial liquid loading to be

$$\psi_{liq} = 6.32 \times 10^{-4} \quad (C5)$$

$$L_{p,max}^* = 0.00036$$

6

7 C.2. LoD based on a Predefined Domain-Averaged Deposition Rate

8 Again, we assumed that $\rho_v \approx 0$ and that the system is at a quasi-steady state. We then
 9 assumed that $\dot{m}_{dep} = 0.1 \dot{m}_{injection} / N_p$, i.e., 10% of the injected droplets are deposited
 10 uniformly-distributed on the particles. This assumption is based on the results of primary
 11 simulation we performed. By adopting Kariuki's model, we arrive at:

$$\psi_{liq} = \frac{\dot{m}_{dep}}{A_p \beta_p \rho^{eq}} = \frac{0.1 \dot{m}_{inj} / N_p}{\pi d_p D_{vap} sh \rho^{eq}} = 4.3 \times 10^{-7} \quad (C6)$$

$$L_{p,max}^* = 2.49 \times 10^{-7}.$$

12

1 C.3. LoD based on a Predefined Surface Coverage

2 By using Kariuki's model, it is straight forward to compute the liquid loading level. Thus, for
3 a coverage of 50% we arrive at

$$L_{p,max}^* = 0.395 \quad (C7)$$

4 C.4. Relationship between of Surface Coverage and Particle Liquid Content for 5 Kariuki's Model

6 The surface coverage of particle in the model developed by Kariuki et al. ²⁸ is given by

$$\psi_{liq} = 1 - [1 - f]^{\Phi_p/f} \quad (C8)$$

7 Where parameter f is fraction of particle surface coated by a single droplet, and Φ_p is the
8 particle coating number given by

$$f = \frac{A_{d,projected}}{A_p} = \frac{\pi d_d^2}{\pi d_p^2} = \left(\frac{d_d}{d_p}\right)^2 \quad (C9)$$

$$\Phi_p = N_d f \quad (C10)$$

9 Here N_d is the number of deposited droplets, which can be calculated as

$$N_d = \frac{V_{d,total}}{V_d} = \frac{V_p L_p^*}{V_d} \quad (C11)$$

10 By inserting this definition into the original model, we arrive at

$$\psi_{liq} = 1 - [1 - f^2]^{\frac{V_p L_p^*}{V_d}} = 1 - e^{\left[\ln(1-f^2) \frac{V_p L_p^*}{V_d}\right]} \quad (C12)$$

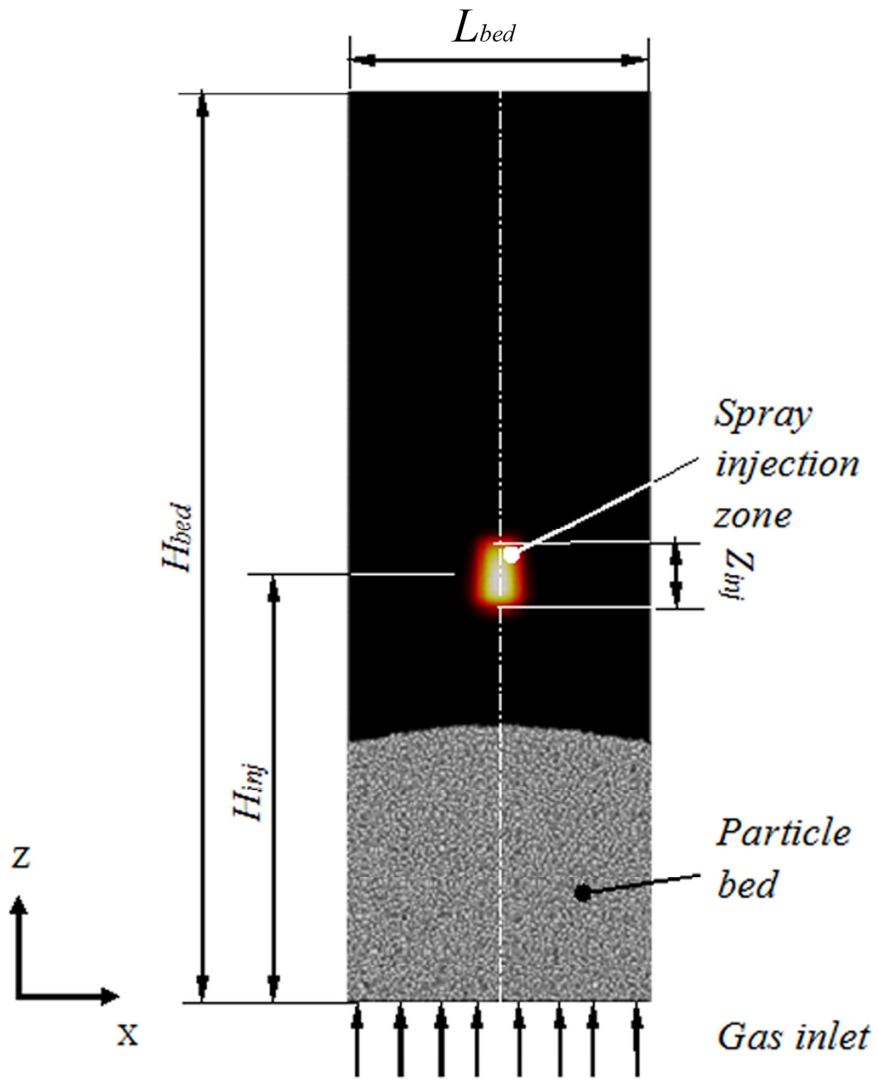
11 By rewriting this equation, we now isolate L_p^* as

$$L_p^* = \frac{V_d \ln[1 - \psi_{liq}]}{V_p \ln\left[1 - \left(\frac{d_d}{2d_p}\right)^2\right]} \quad (\text{C13})$$

1

2

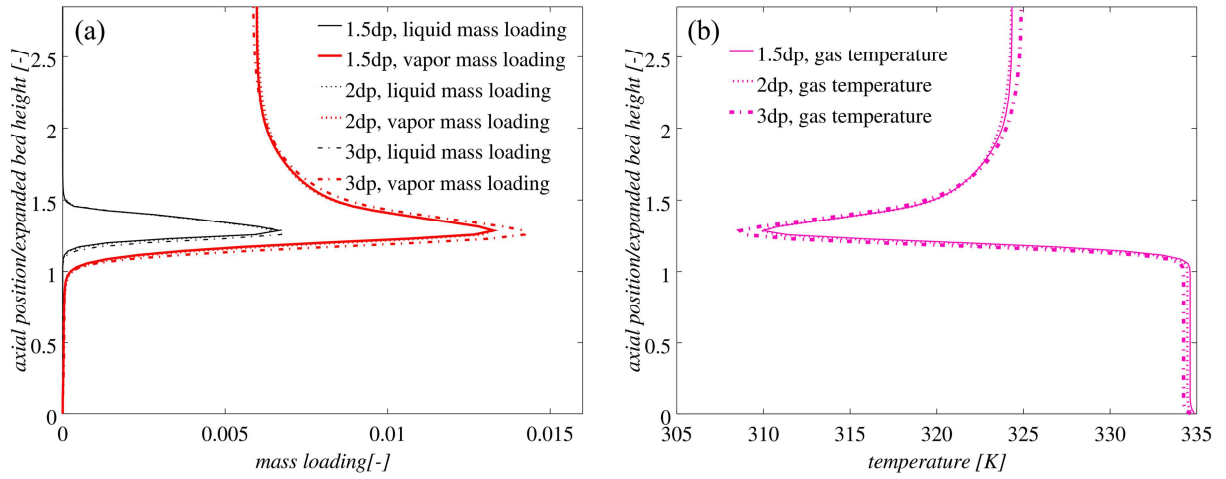
1 **Figures**



2

3 Fig. 1. Schematic setup used for the simulation

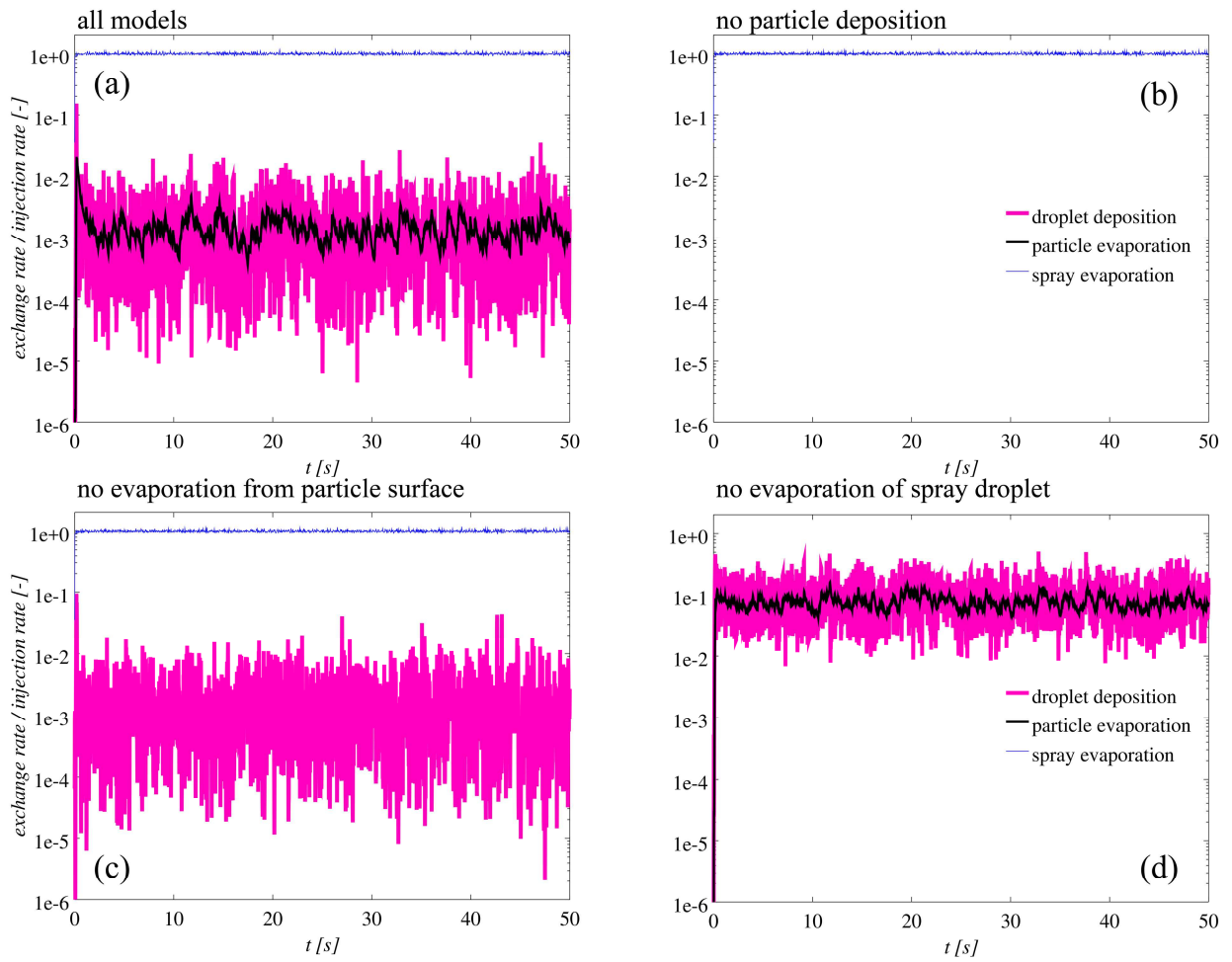
4



1

2 Fig 2. Comparison of time-averaged a) mass loadings and b) temperatures along the bed
 3 for various grid sizes (data is taken from $x = 7$ [mm], i.e., at the center of the bed).

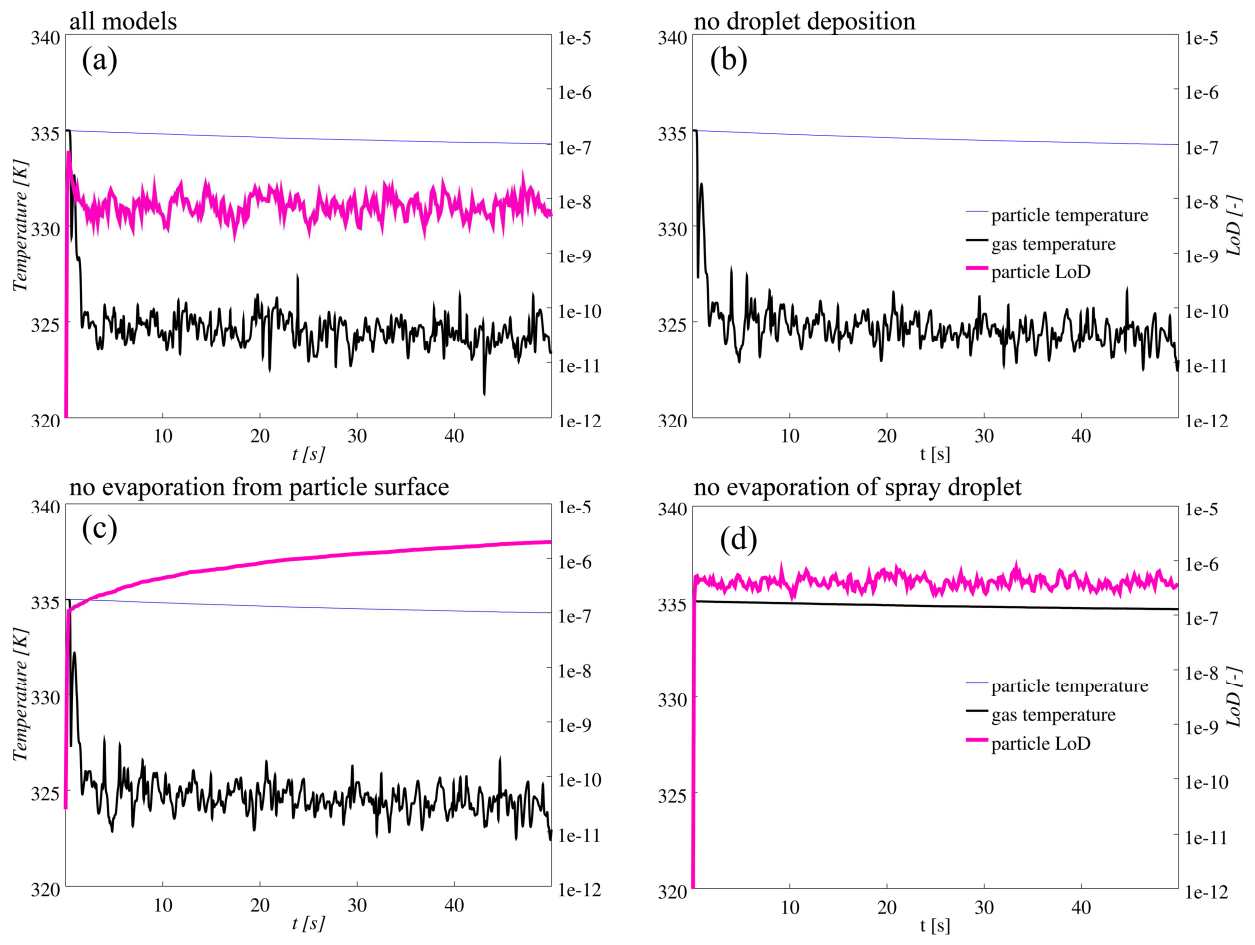
4



1

2 Fig. 3. Comparison of exchange rates for cases with a) all models (case A), b) no droplet
 3 deposition (case B), c) no particle evaporation (case C), and d) no evaporation from
 4 droplets in the spray (case D).

5



1

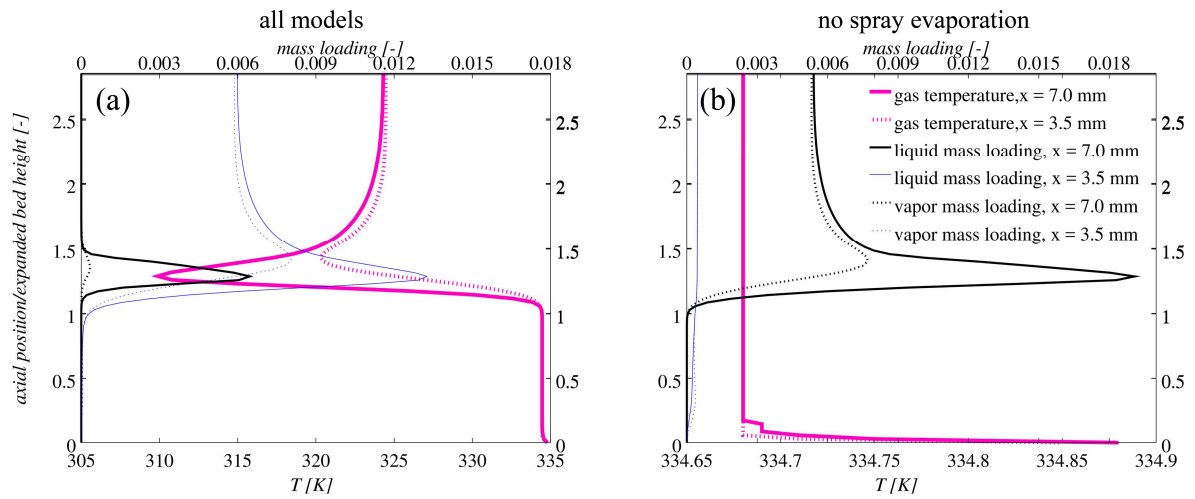
2

3

4

5

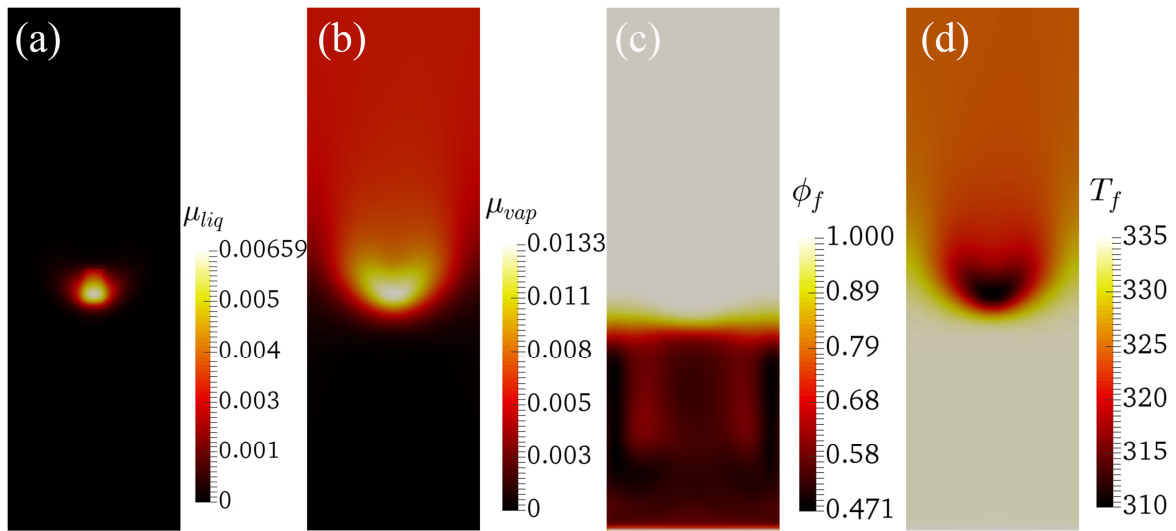
Fig. 4. Comparison of mean particle temperature and LoD as well as gas outlet temperature for cases with a) all models (case A), b) no droplet deposition (case B), c) no particle evaporation (case C), and d) no droplet evaporation (case D).



1

2 Fig.5 Comparison of time-averaged gas temperatures and mass loadings along the bed
 3 for cases with a) all models and b) no droplet evaporation.

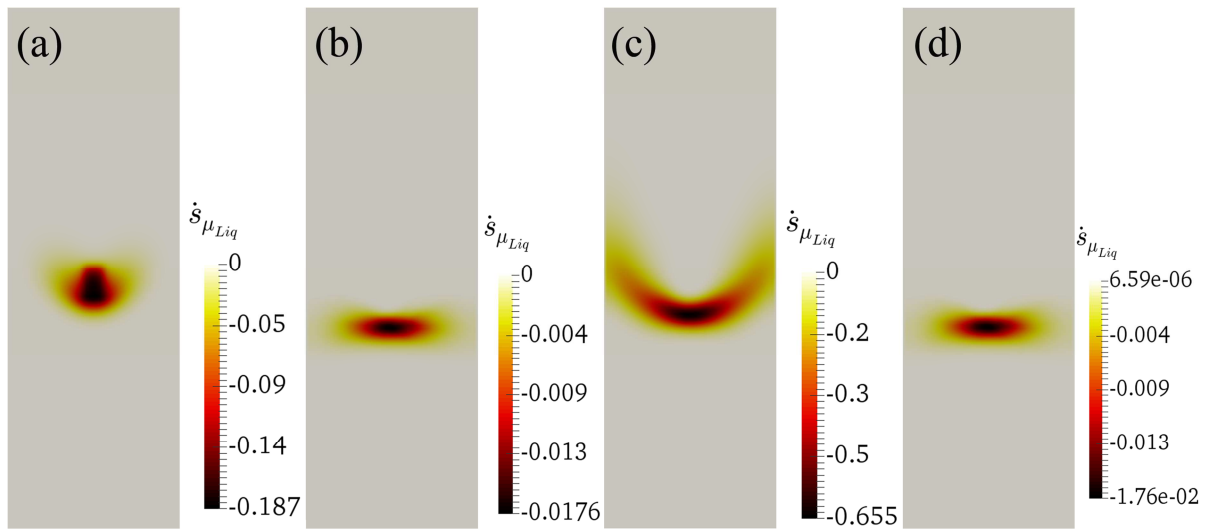
4



1

2 Fig.6. Predicted contour plot at the bed cross section at Y=0 for a-d) scalar quantities in
 3 case A (i.e., using all models; a: liquid mass loading, b: vapor mass loading, c: voidage, d:
 4 gas temperature),

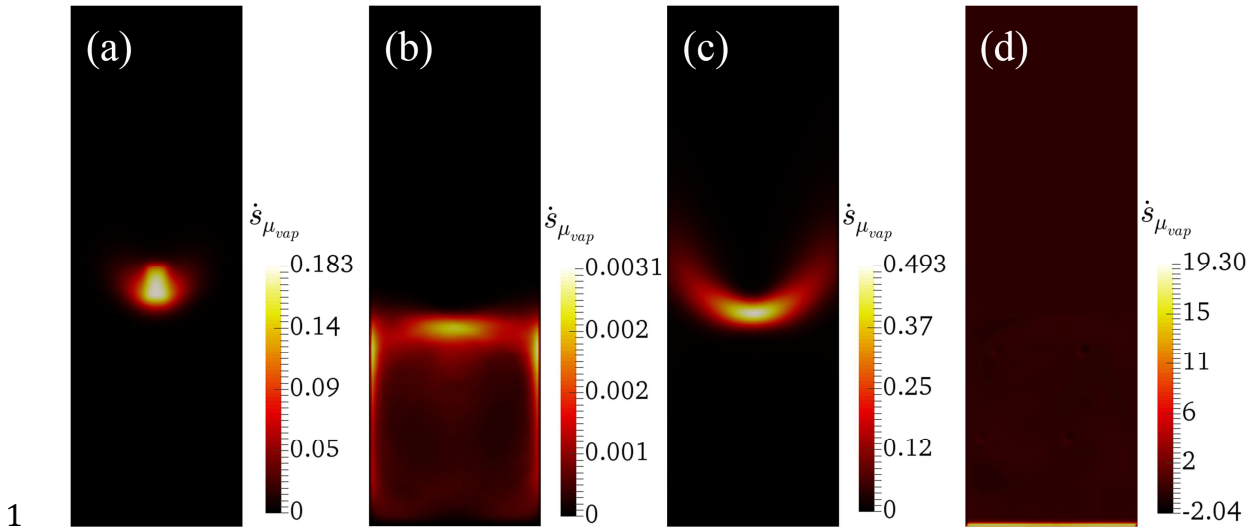
5



1

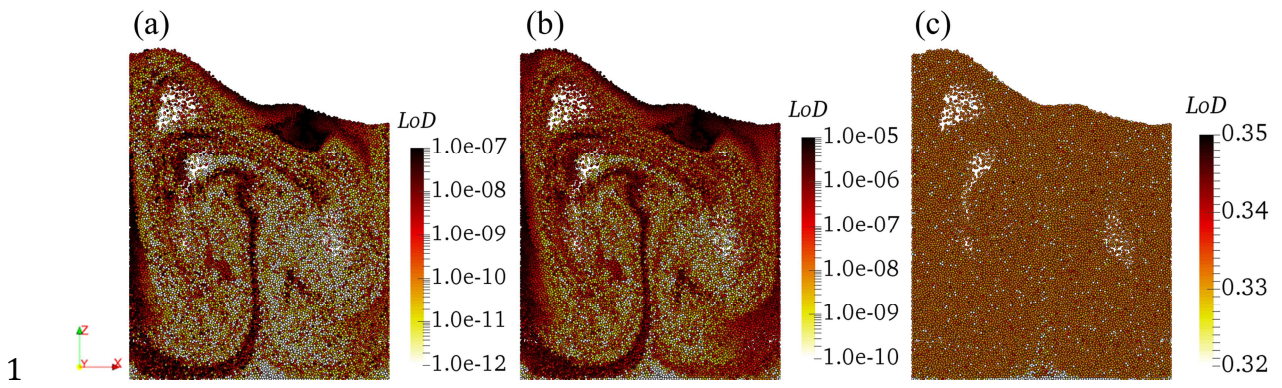
2 Fig.7. Predicted contour plot at the bed cross section at $Y=0$ for liquid exchange rates for
 3 cases with 1) all models, 2) no droplet evaporation, 3) highest injection rate, and 4)
 4 highest initial LoD (all data shown is time-averaged).

5



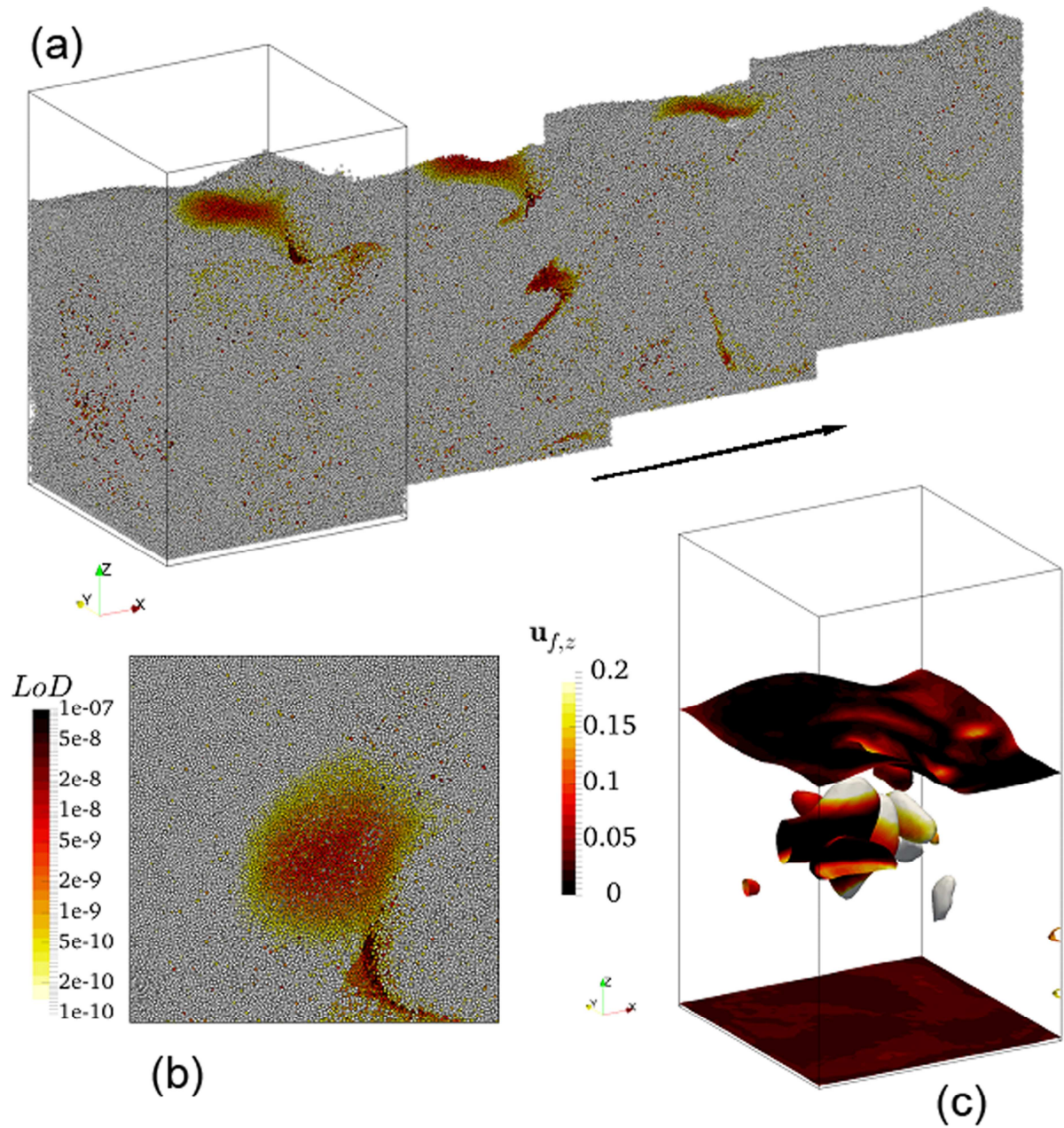
1
 2 Fig.8. Predicted contour plot at the bed cross section at $Y=0$ for vapor exchange rates for
 3 cases with 1) all models, 2) no droplet evaporation, 3) highest injection rate, and 4)
 4 highest initial LoD (all data shown is time-averaged).

5



1
2 Fig. 9. Instantaneous particle liquid content for cases with a) all models (case A), b) no
3 droplet evaporation (case D), and c) initial surface coverage of 0.5

4

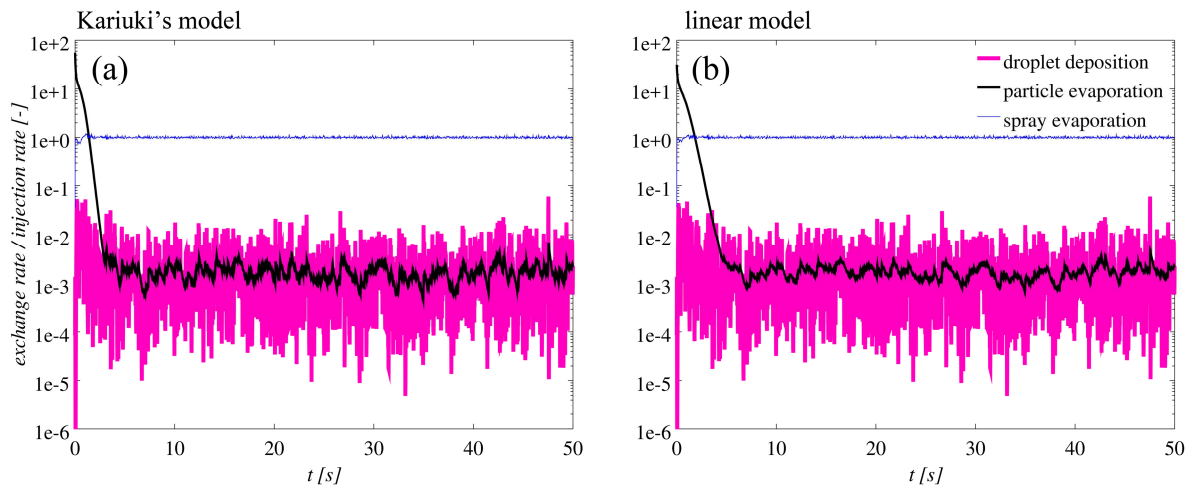


1

2 Fig. 10. Instantaneous particle liquid content for the 3D case for a) a sliced-up version of
 3 the 3D simulation, b) a top view, and c) isocontours of at $\phi_f = 0.8$ colored by the fluid's
 4 vertical speed).

5

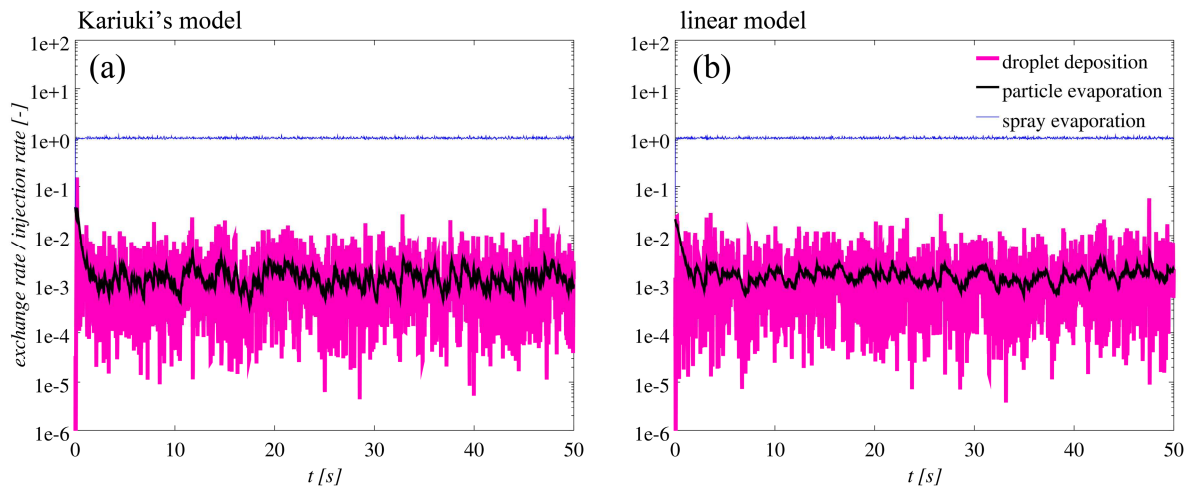
6



1

2 Fig. 11. The predicted exchange rates using maximum averaged initial LoD for a)
 3 Kariuki's Model and b) linear model.

4

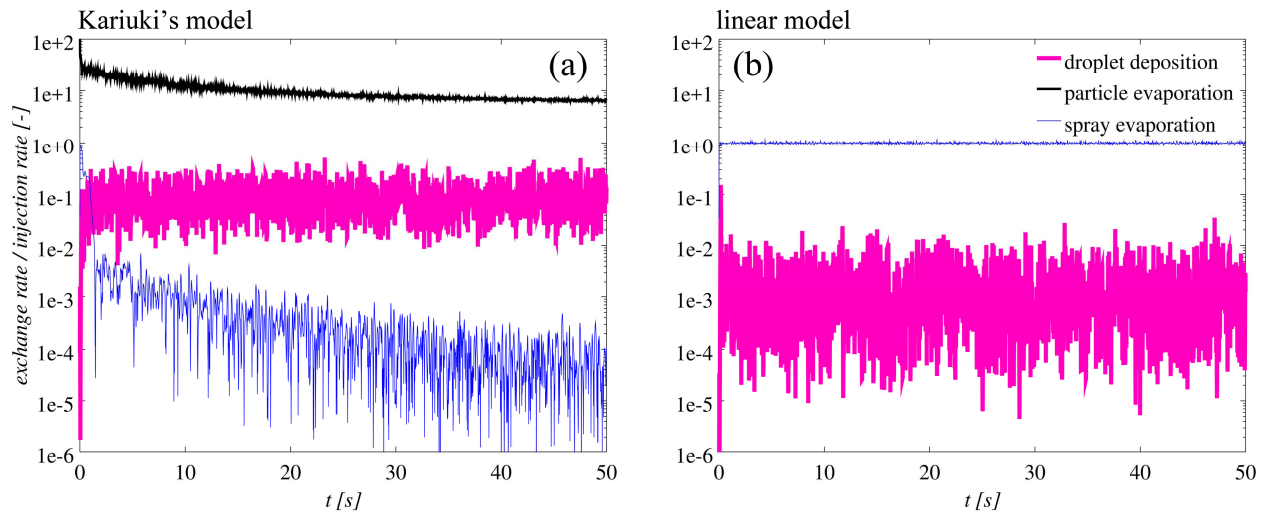


1

2 Fig. 12. The predicted exchange rates using mean initial LoD for a) Kariuki's Model, b)

3 Linear Model.

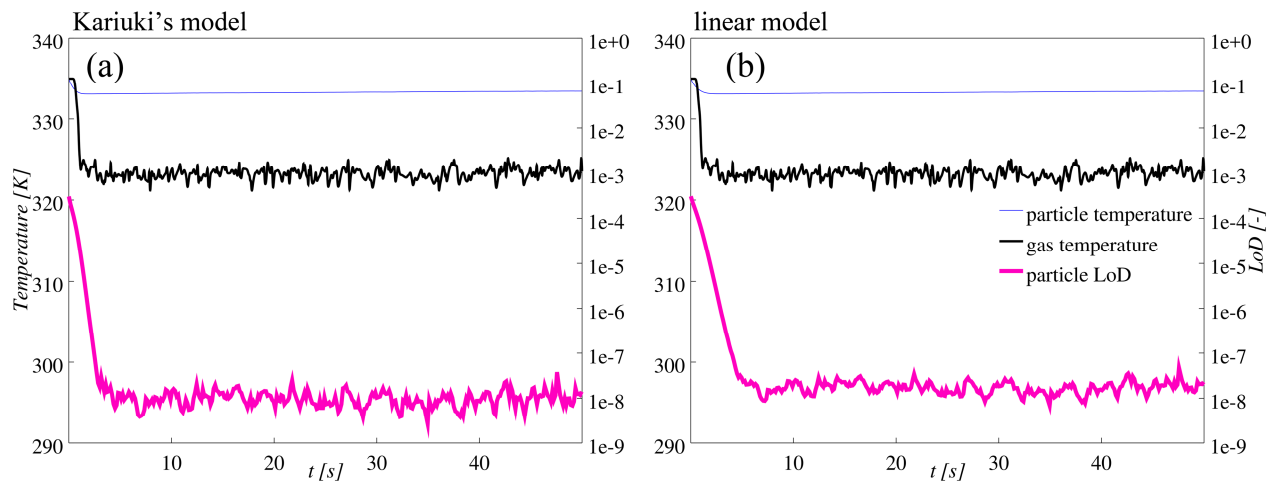
4



1

2 Fig. 13. The predicted exchange rates using Initial LoD corresponding to surface
 3 coverage of 0.5 for a) Kariuki's Model, b) Linear Model.

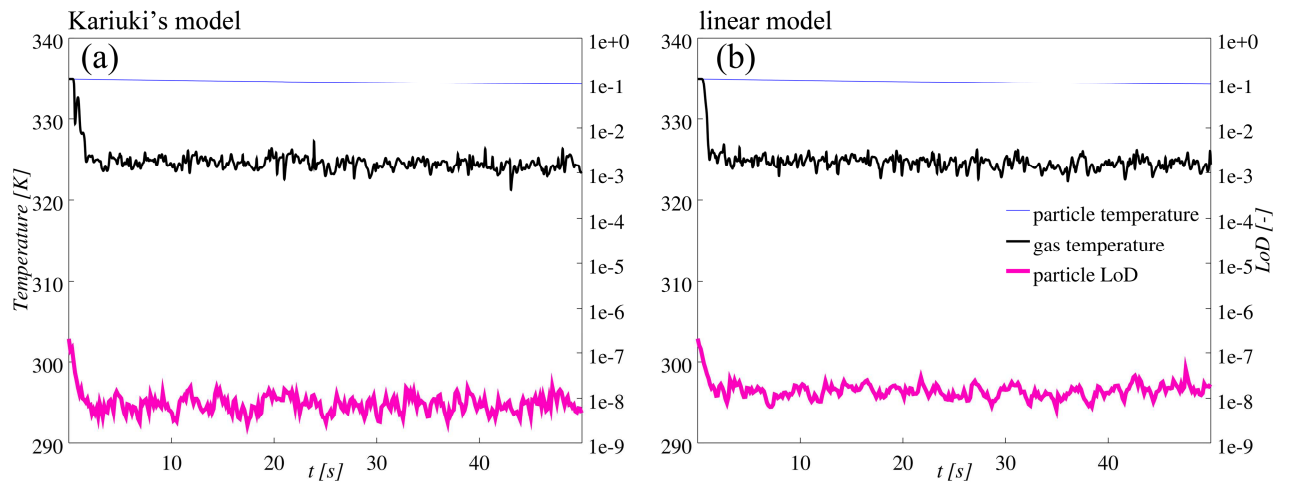
4



1

2 Fig. 14. The predicted temperature and LoD using maximum averaged initial LoD for a)
 3 Kariuki's Model and b) linear model.

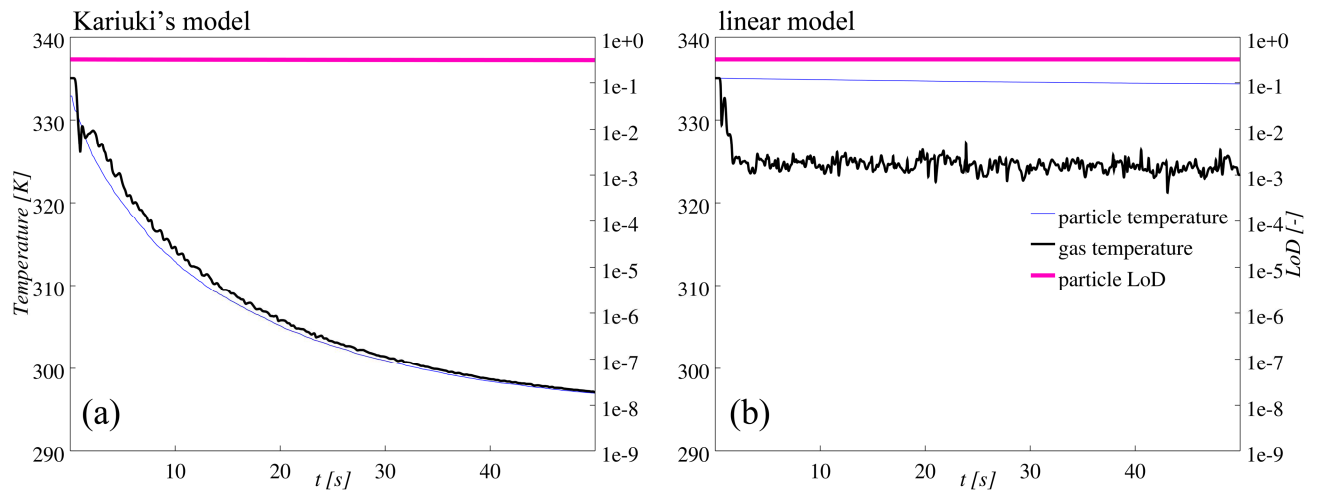
4



1
2

3 Fig. 15. The predicted temperature and LoD using mean initial LoD for a)Kariuki's
4 Model, and b) Linear Model.

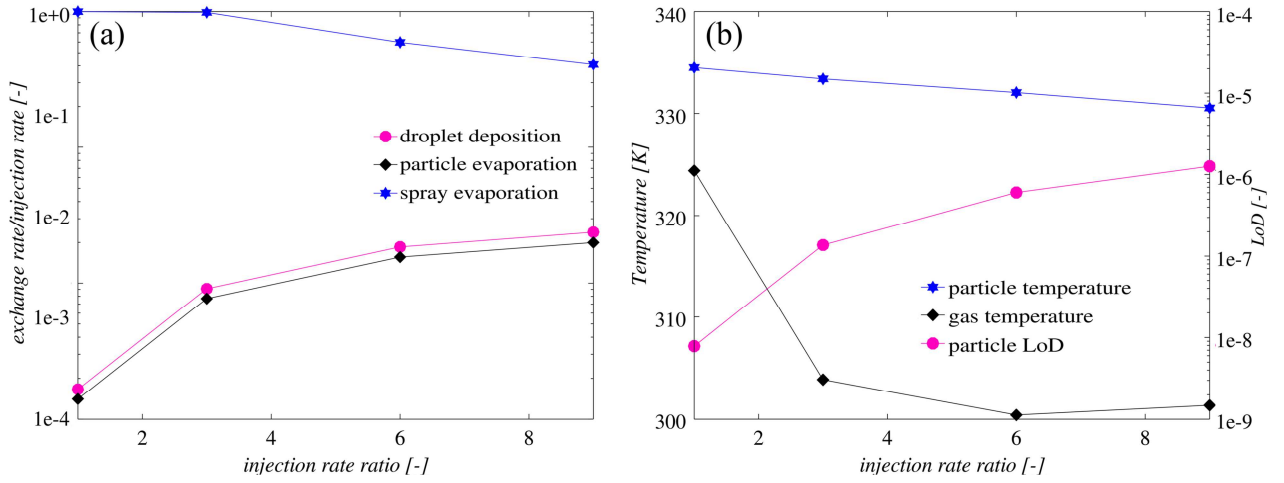
5



1

2 Fig. 16. The predicted temperature and LoD using mean initial LoD corresponding to
 3 surface coverage of 0.5 for a) Kariuki's Model, and b) Linear Model

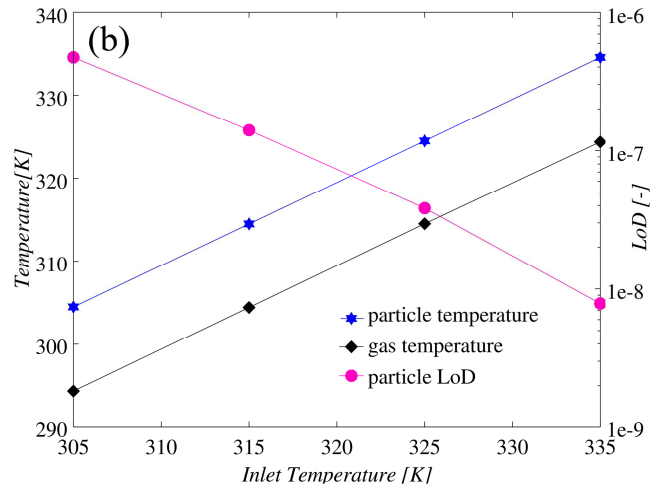
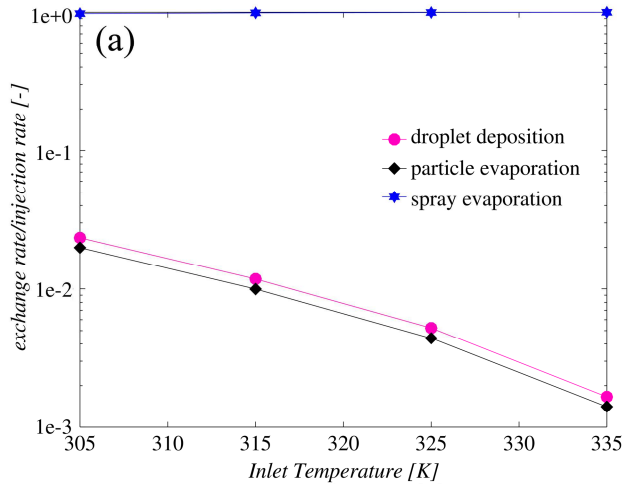
4



1

2 Figure 17. The effect of the liquid injected rate on the normalized exchange rates (panel
 3 a), the gas and particle temperatures, as well as the LoD (panel b)

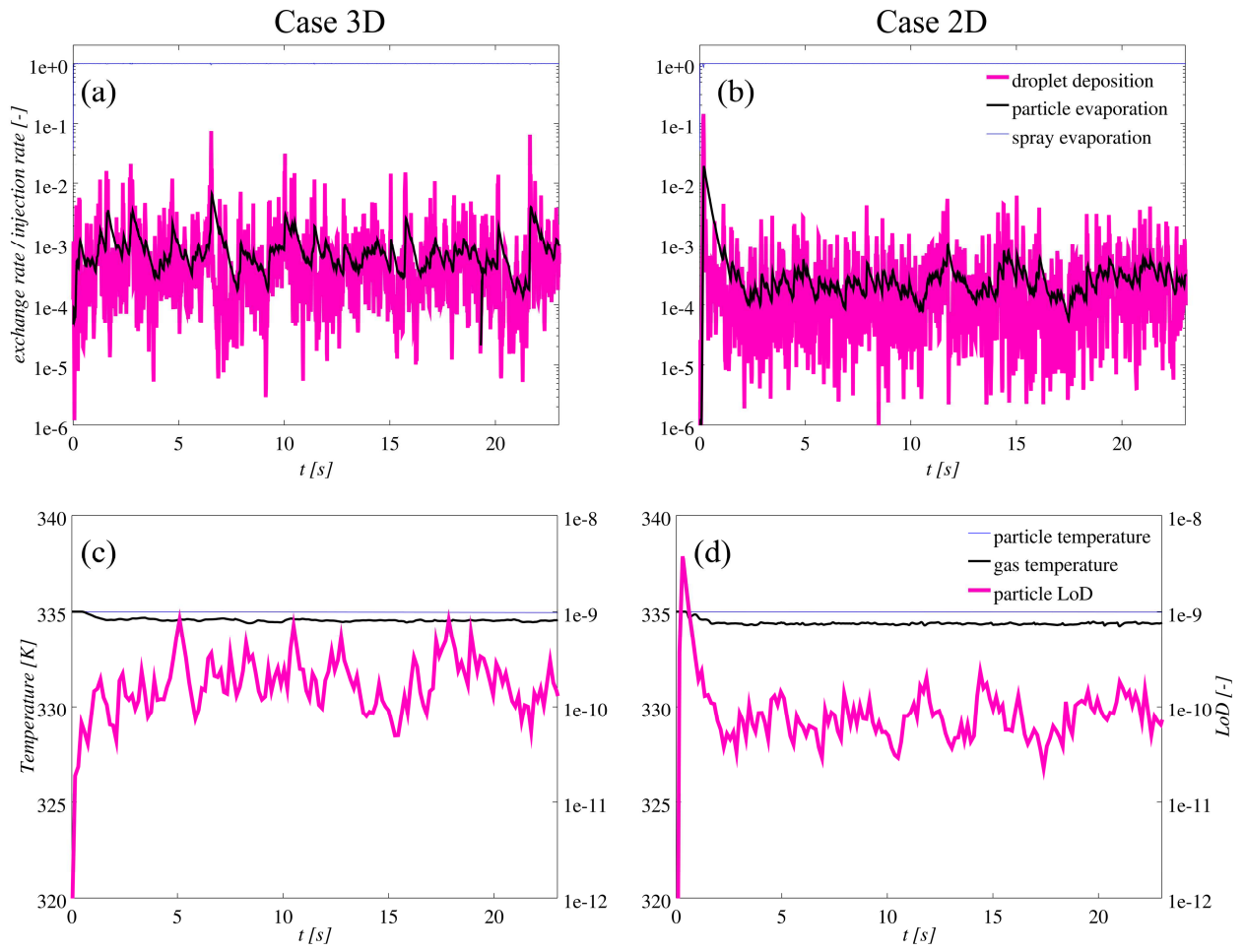
4



1

2 Figure 18. The effect of the inlet temperature on the normalized exchange rates (panel
 3 a), the gas and particle temperatures, as well as the LoD (panel b).

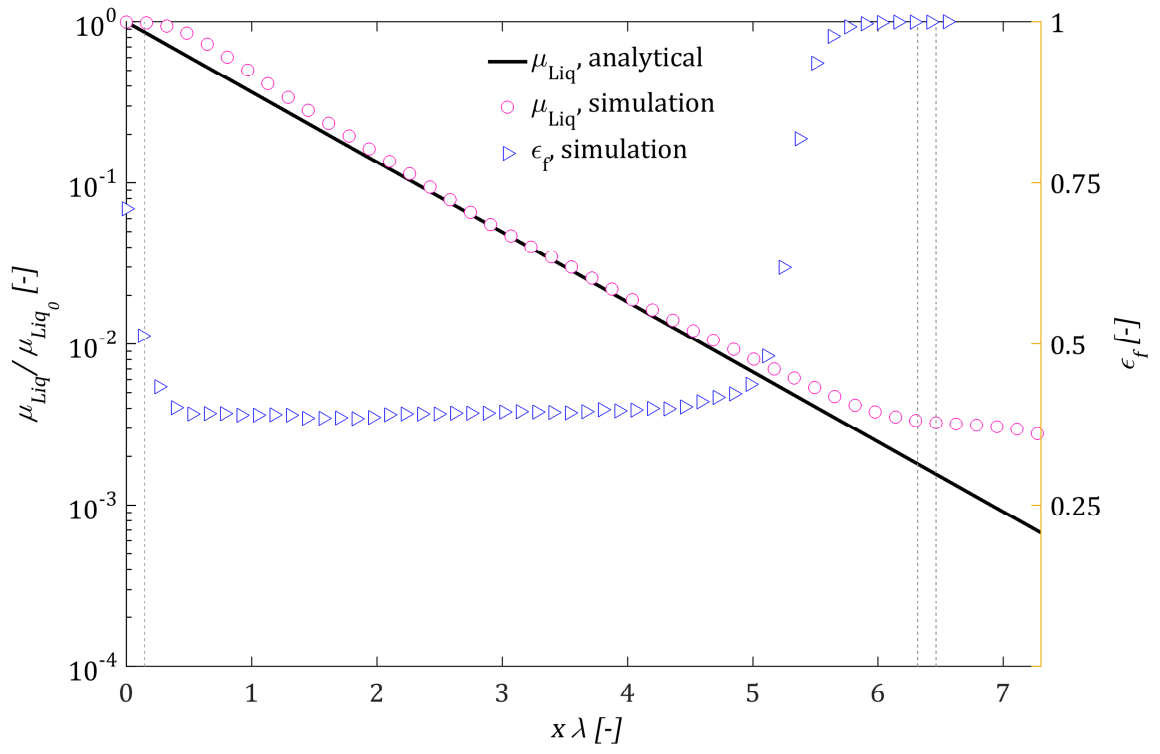
4



1

2 Figure 19. a) 3D simulation results for the normalized exchange rates b) 2D simulation
 3 results for the normalized exchange rates c) LoD and temperatures for 3D case d) LoD
 4 and temperatures for 2D case.

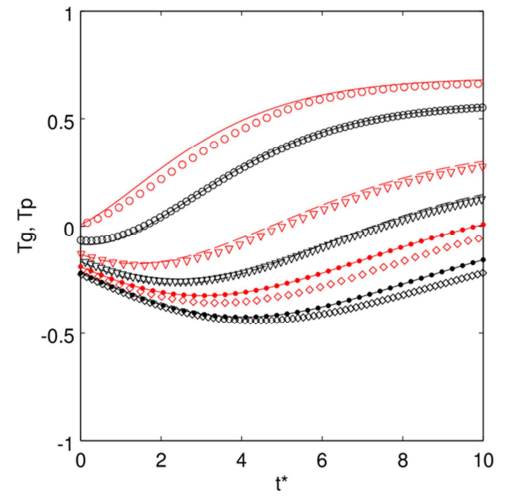
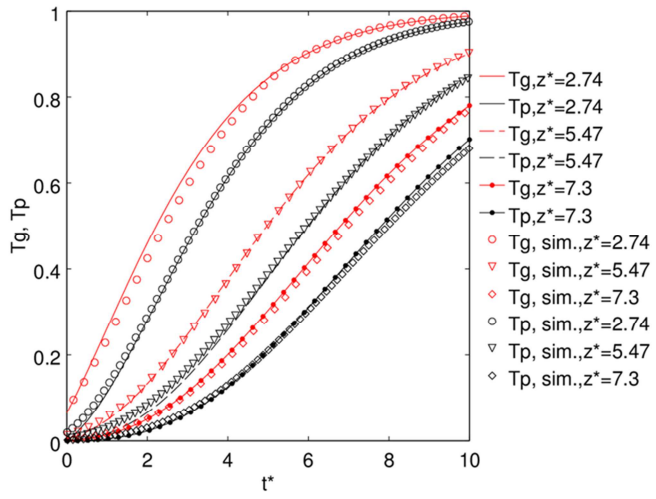
5



1

2 Figure A.1

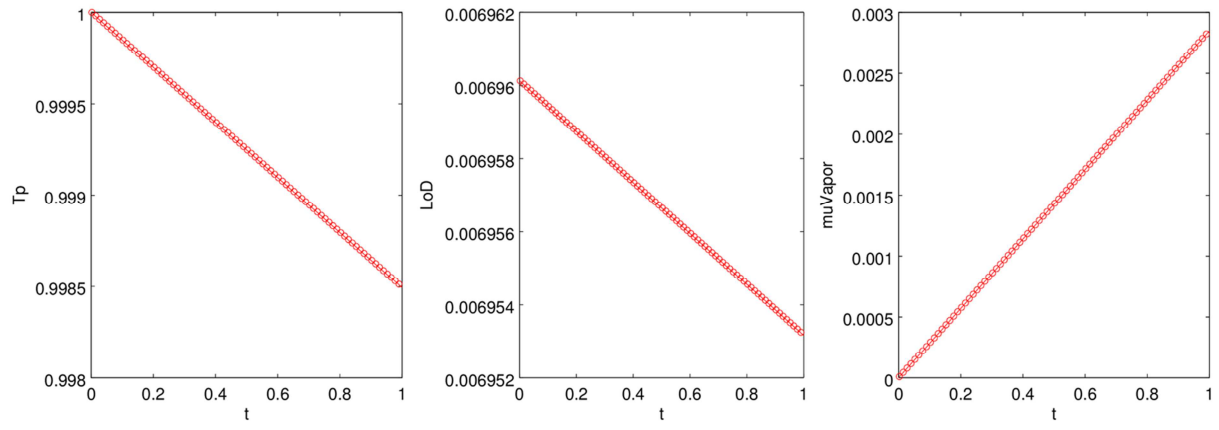
3



1

2 Figure A.2

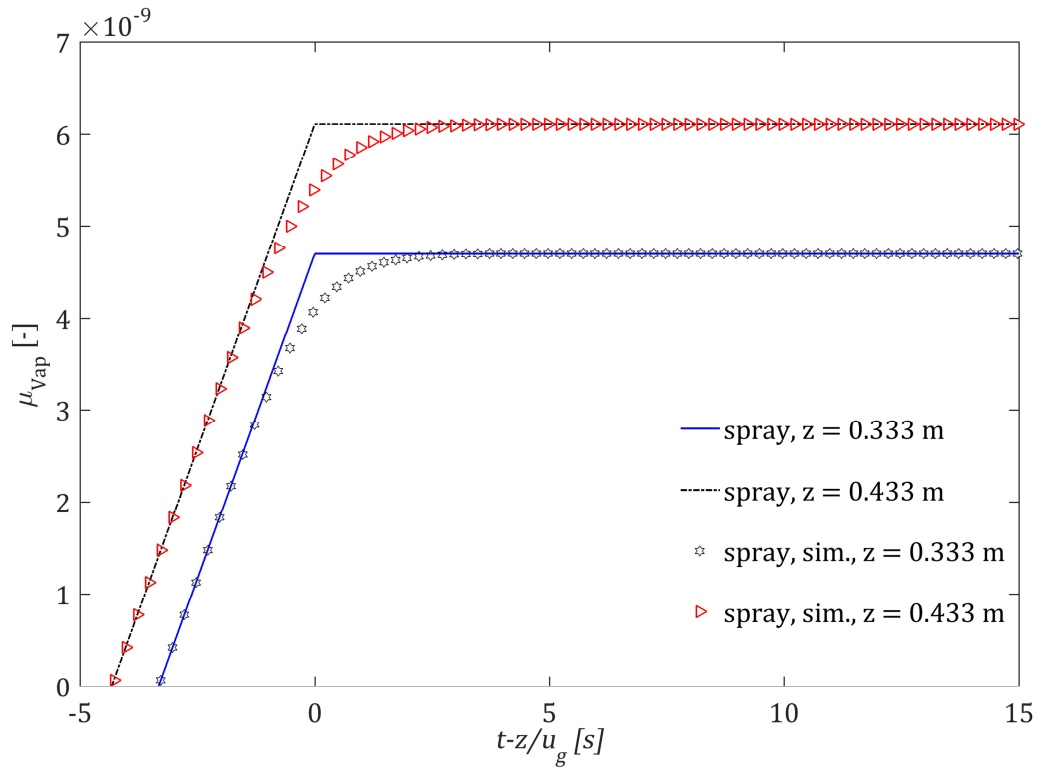
3



1

2 Figure A.3

3



1

2 Figure A.4

3